4 Effects of High Salinity PWRI Practice on Sulfidogenesis and Microbially Influenced Corrosion

Mohammed Sindi and Xiangyang Zhu
Saudi Aramco, Dhahran, Saudi Arabia

Beate Christgen
Newcastle University, Newcastle upon Tyne, United Kingdom

Angela Sherry
Northumbria University, Newcastle upon Tyne, United Kingdom

Neil Gray
School of Natural and Environmental Sciences (SNES), Newcastle University, Newcastle upon Tyne, United Kingdom

Ian Head
Newcastle University, Newcastle upon Tyne, United Kingdom

4.1 INTRODUCTION: BACKGROUND AND DRIVING FORCES

Microbially influenced corrosion is a global issue influencing the premature failure of metallic infrastructure and accounting for 20% of all internal corrosion incidences (Zhu, *et al*., 2003). Numerous microorganisms are implicated in MIC including sulphate-reducers, methanogens, nitrate-reducers, iron-oxidisers, iron-reducers, and acid-producers. The aim of this chapter was to explore the effects of high salinity (127 g/L TDS; 204 g/L TDS) in a range of temperature incubations (15°C, 30°C,

DOI: 10.1201/9781003287056-7

45°C, and 60°C) resulting from and simulating the mixing of synthetic injected seawater (ISW) and synthetic PW on sulfidogenesis, and the underpinning fundamental processes associated with it such as sulphate reduction into sulphide, microbial community composition, and MIC. This wide range of incubating temperatures and high salinity ISW:PW mix represents plausible ISW, and PW thermal gradient encountered under different oil and gas industry operational settings including: A) On-shore Oil Production Facility Water Flooding Lines; B) On-shore Oil Production Facility ISW:PW Mixing Tanks; C) Drilling muds (i.e., mixed with a variety of water types including: ISW, PW, Utility Water, etc.) Mixing Tanks; D) Off-shore Platforms ISW:PW Mixing Tanks; and E) Oil Reservoir ISW:PW Mixing Zone.

Production Water for Reinjection practices are commonly utilised in the oil and gas industry. Additionally, seawater injection and PWRI lead to in-reservoir salinity gradients from seawater salinity (35 g/L TDS) at the injector, to the usually higher formation water salinity within the reservoir. Injection of cool seawater also leads to the formation of a temperature gradient with a significant impact on the growth and activity of microorganisms in petroleum reservoirs. A specific high salinity PWRI practice of 20% synthetic ISW mixing with 80% synthetic PW from the North Sea (NS) (127 g/L TDS) and the AG (204 g/L TDS) production water systems were selected for the following reasons:

A) As a result of synthetic (ISW:PW) mixing, the sulphate concentration will decrease from 21 mM in 100:0% ISW:PW(NS) to approximately 0.6 mM in 0:100% ISW:PW(NS), affecting the growth and activity of SRP.
B) At this (20:80%) ISW:PW (NS-127 g/L TDS) salinity from the previous work conducted by Sindi, *et al*. (2021), a shift from the SRP enrichments of *Desulfobacter* sp., *Desulfotignum* sp., and *Desulfobulubus* sp., observed under 100% ISW (NS) (42 g/L TDS), into members of endospore-formers *Peptococcaceae* family, and *Halanaerobium* sp., (sporulation, thiosulfate reduction, and/or fermentation metabolism) observed under the aforementioned high salinity 20:80% ISW:PW (NS) (127 g/L TDS) was evident.
C) These (20:80%) ISW:PW (NS – 127 g/L TDS; AG – 204 g/L TDS) mixes, therefore, represent the highest salinities with noticeable sulphate (mM) concentrations available for anaerobic sulphate respiration by SRP: (20:80% ISW:PW (NS) 5 mM sulphate; (20:80% ISW:PW (AG) 10 mM sulphate).
D) Considering the aforementioned reasons of (20:80% ISW:PW) being the highest in salinity mix with noticeable sulphate (mM) concentrations available for anaerobic sulphate respiration by SRP, and the observed microbial community successions at this higher salinity from the previous work conducted by Sindi, *et al*. (2021) (i.e., sulphate reduction – sporulation, thiosulfate reduction and/or fermentation), it was thought to be interesting to evaluate the MIC potential under such high salinity (ISW:PW) mixes and across a thermal gradient that represented plausible oil and gas industry operational settings.

Therefore, developing fundamental insights on the impact of high salinity PWRI mixing practices on microbial processes, microbial communities, and MIC will help inform knowledge-driven best field practices for PWRI, and other microbially

implicated processes such as hydraulic fracturing and drilling, where also this high salinity PWRI or similar water mixing procedures will occur.

4.2 SUMMARY OF METHODS

4.2.1 Incubations

Microcosms were setup by inoculating the bicarbonate, trace elements, vitamin mixture basal mineral media (Widdel and Bak, 1992) with 5% w/v inoculum. Based on the selected NS and the AG mixing scenarios, all ISW:PW microcosms had sulphate as the main electron acceptor (21 mM, 10 mM, and 5 mM), and a mixture of volatile fatty acids (VFA: 10 mM acetate, 10 mM propionate, and 5 mM butyrate) used as electron donors, and the five basal salts (NaCl, $CaCl_2.2H_2O$, $MgCl_2.6H_2O$, KCl, and Na_2SO_4) calculated based on the average cationic and anionic compositions of Na, K, Cl, SO_4, and Mg from 52 producing wells in the NS (Bjørlykke, 1995), and five producing wells from the United Arab Emirates (U.A.E), the Kingdom of Saudi Arabia (KSA), and Kuwait (Bader, 2007). As a result, different ISW:PW salinity mixes (%) of 42 g/L TDS, 127 g/L TDS, and 204 g/L TDS were generated (Table 4.1). Each ISW:PW salinity mix (%) treatment condition microcosms were prepared in triplicates in 200 ml Wheaton bottles (190 ml final culture volume), (80 mm × 10 mm × 1 mm) of cleaned 0.2% carbon steel coupons in plastic fittings (Lahme, *et al*., 2019), closed with butyl rubber stoppers, crimped sealed with aluminium caps, and the headspace flushed with (CO_2/N_2) (20:80%). Three treatment conditions had no corrosion coupon additions in them and were: 100% ISW (NS) (42 g/L TDS), 20:80% ISW:PW (NS) (127 g/L TDS), and 20:80% ISW:PW (AG) (204 g/L TDS), and that the 100% ISW (NS) (42 g/L TDS) treatment condition was used as a positive control for sulfidogenesis (Table 4.1). All treatment conditions and controls microcosms were incubated horizontally for the corrosion coupons to be completely submerged in the ISW:PW solution for the corrosion process to initiate. Additionally, all microcosms were anaerobically incubated at 15°C, 30°C, 45°C, and 60°C, except

TABLE 4.1
Treatment Conditions and Controls in ISW:PW Anaerobic Microcosms across the Salinity and Temperature Gradients

Mixed Ratios of ISW:PW (%)	Incubating Temperature (°C)				Treatment Rationale	Replication	Final Sulphate (mM)	Final Salinity (g/L)
100% ISW (∅)	30				* A	3	21	42
20:80% ISW:PW (∅) (NS)	30				* A		4.6	127
20:80% ISW:PW (∅) (AG)	30				* A		9.8	204
20:80% ISW:PW (∇) (NS)	15	30	45	60	* B		4.6	127
20:80% ISW:PW (∇) (AG)	15	30	45	60	* B		9.8	204

* A (Sulfidogenesis only analysis)
* B (Salinity and temperature interactions (Full-scale analyses)
(∇) (Corrosion coupons added), (∅) (Corrosion coupons not added); NS (The North Sea); and AG (The Arabian Gulf); ISW (Injected Sea water); and PW (produced water).

for the no coupon incubations which were incubated only at 30°C and resulting in 11 different treatment conditions.

Three no coupon ISW:PW anoxic microcosms were set up for sulfidogenesis analysis (Table 4.1). The sulfidogenesis positive control (100% ISW) (30°C), 20:80% ISW:PW (NS) (127 g/L TDS), and 20:80% ISW:PW (AG) (204 g/L TDS), without coupon incubations, were set up (Table 4.1). Additionally, the following eight anoxic ISW:PW microcosms incubated with corrosion coupons were set up: (20:80 ISW:PW) (127 g/L TDS) (15°C-NS), (20:80 ISW:PW) (127 g/L TDS) (30°C-NS), (20:80 ISW:PW) (127 g/L TDS) (45°C-NS), (20:80 ISW:PW) (127 g/L TDS) (60°C-NS), (20:80 ISW:PW) (204 g/L TDS) (15°C-AG), (20:80 ISW:PW) (204 g/L TDS) (30°C-AG), (20:80 ISW:PW) (204 g/L TDS) (45°C-AG), and (20:80 ISW:PW) (204 g/L TDS) (60°C-AG) (Table 4.1).

4.2.2 Analytical Procedure

The ISW:PW treatment conditions were sampled for a period of approximately 7.5 months to 225 days). The concentration of sulphate was measured using an Ion Chromatography method; using column (AS14A), the autosampler (AS40), a Dionex Cd-25 Conductivity Detector Model 1S25 Na_2CO_3 (8mM)/$NaHCO_3$ (1 mM) as eluent, at 1ml/min flow rate, and 25 µL injection loop, nitrogen gas as the carrier at 9 psi, unicam 4851 integrator, and chromatograms visualised using the Chameleon Dionex Software. Aqueous sulphide was measured spectrophotometrically at 480 nm following the reaction of aqueous sulphide with 5 mM $CuSO_4$ in 50 mM HCl solution, to produce a brown CuS precipitate (Cord-Ruwisch, 1985). Sulphate reduction (mM), sulphide production/depletion (mM), and sulphide depletion rates (mM/hrs.) were compared statistically by One-Way Analysis of Variance (ANOVA; Minitab 17, Minitab Ltd., Coventry, UK). Headspace methane was measured following Gas Chromatography using Flame Ionisation Detector (GC-FID) instrument. Gravimetric analysis and corrosion rates were conducted to determine corrosion coupons weight loss in grams (g) and to calculate corrosion rates in millimetres per year (mm/yr), as described elsewhere (Enning, *et al*., 2012). Surface characterisation of the corrosion coupons was conducted using the Tescan Vega 3LMU scanning electron microscope fitted with a Bruker XFlash® 6 | 30 detector for EDS analysis.

4.2.3 DNA Sequencing and Bioinformatics

Two time-series (hrs.) of 0 hrs. and 5400 hrs. (225 days) were selected for DNA extractions for River Tyne sediment inoculum, 20:80% ISW:PW (NS), and 20:80% ISW:PW (AG) (15°C, 30°C, 45°C, and 60°C) incubations. River Tyne estuarine sediments from the day of sample collection were stored in −20°C and were submitted for sequencing as the negative control for the (20:80% ISW:PW) mix samples. DNA sequencing was carried out at Northumbria university (NU-OMICS) on MiSeq (illumina platform), and *16S rRNA* sequence libraries were analysed using Quantitative Insights into Microbial Ecology 2 (QIIME2) and Statistical Analysis of Metagenomic Profiles (STAMP) software packages. STAMP v2.1.3 (Parks, *et al*., 2014) was used to determine the overall species level Amplicon Sequence Variants (ASVs) clustering

patterns of ISW:PW microcosms across the salinity and temperature gradients (using Principal Component Analysis (PCA)) and generating time-series (hrs.) phylum/order level heatmaps across the salinity and temperature gradients.

4.3 RESULTS

4.3.1 Effects of High Salinity PWRI Practice on Sulfidogenesis and Sulphate Reduction

Sulphide monitoring revealed a systematic sulphide depletion profile for both 20:80% (ISW:PW) (NS) (127 g/L TDS) and 20:80% ISW:PW (AG) (204 g/L TDS) (with coupon incubations) (15°C–60°C) (Figure 4.1), a minute sulphide production for 20:80% (ISW:PW) (NS) (127 g/L TDS) (no coupon incubation), and negligible sulphide production for 20:80% ISW:PW (AG) (204 g/L TDS) (no coupon incubation) (Figure 4.2), all compared with 100% ISW (30°C) (no coupon incubation) (Figures 4.1 and 4.2).

For the psychrophilic temperature incubations (15°C), in microcosms containing (20:80%) ISW:PW (NS) (127 g/L TDS), a high sulphide depletion of 2.64 mM ± 0.003 was observed. With increasing temperature in the mesophilic temperature incubations (30°C), in microcosms containing (20:80%) ISW:PW (NS) (127 g/L TDS), sulphide depletion decreased to 2.48 mM ± 0.10 (Figure 4.1). With further increase in temperature in the lower thermophilic incubations (45°C), in microcosms containing (20:80%) ISW:PW (NS) (127 g/L TDS), higher sulphide depletion of 2.80 mM ± 0.08 was observed (Figure 4.1). The highest sulphide depletion

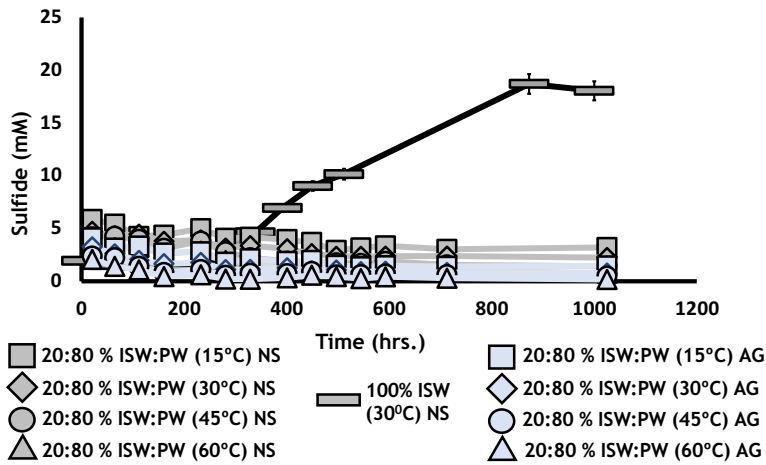

FIGURE 4.1 Sulfidogenesis profiles across the ISW:PW mixes (%) for the temperature gradient of (15°C, 30°C, 45°C, and 60°C) incubations. Symbols with grey lines depict 20:80% ISW:PW (NS) (127 g/L TDS) conditions (with corrosion coupons). Blue symbols and lines depict 20:80% ISW:PW (AG) (204 g/L TDS) (with corrosion coupons). Black line depicts 100% ISW (NS) (42 g/L TDS) (30°C) (without corrosion coupons). Error bars represent 1 × SE.

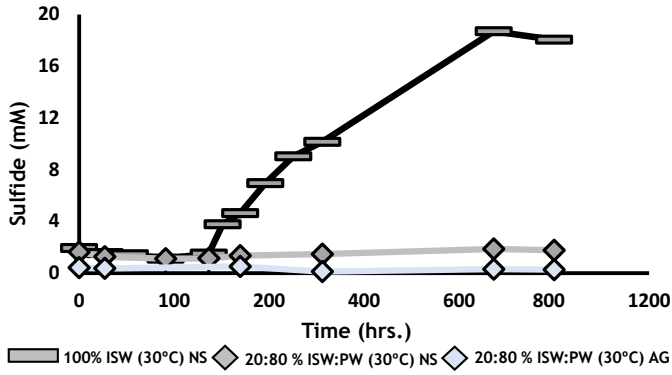

FIGURE 4.2 Sulfidogenesis profiles at 30°C in anoxic microcosms containing 100% ISW (NS), and the ISW:PW mix (%) microcosms from the North Sea and the Arabian Gulf Systems – no coupon incubations. Error bars represent 1 × SE.

of 2.93 mM ± 0.07 was observed under the moderate thermophilic temperature incubations (60°C) in microcosms containing (20:80%) ISW:PW (NS) (127 g/L TDS) (Figure 4.1).

For the psychrophilic temperature incubations (15°C), in microcosms containing (20:80%) ISW:PW (AG) (127 g/L TDS), the highest sulphide depletion of 2.65 mM ± 0.10 was observed. With the increase in incubating temperatures represented in the mesophilic (30°C), lower thermophilic (45°C), and moderate thermophilic (60°C); in microcosms containing (20:80%) ISW:PW (AG) (127 g/L TDS), lower sulphide depletions of 2.49 mM ± 0.06; 1.89 mM ± 0.02; and 1.9 mM ± 0.03, respectively, were observed (Figure 4.1). In contrast, the 100% ISW (30°C) (no coupon incubation) showed a sulphide production rather than depletion of 18.05 mM ± 0.11 (Figure 4.1). One-way ANOVA on Minitab was used as a statistical tool to determine the significance of the sulphide depletion profiles reported for the (NS-PW) system and the (AG-PW) system. This revealed that the differences in sulphide depletion between the (NS-PW) and the (AG-PW) system were non-significant ($P = 0.21$). However, when comparing the sulphide depletion profiles from the (NS-PW) and the (AG-PW) system, with the sulphide production profile reported in 100% ISW (30°C) (no coupon incubation), the statistical tool determined the sulphide production profile was significant ($P = 0.003$).

Next, the sulfidogenesis profiles in no coupon incubations and within the mesophilic incubating temperature (30°C); for both the NS water production system (20:80%) ISW:PW (NS) (127 g/L TDS); and the AG water production system (20:80%) ISW:PW (AG) (204 g/L TDS) were evaluated (Figure 4.2). As illustrated, a minuet sulphide production profile for (20:80% ISW:PW) (30°C – NS) of 1.77 mM ± 0.32 was observed (Figure 4.2), and a negligible sulphide production profile for (20:80% ISW:PW) (30°C- AG) of 0.31 mM ± 0.15 was observed (Figure 4.2). In contrast, the 100% ISW (30°C) (no coupon incubation) showed the highest sulphide production profile of 18.05 mM ± 0.11 (Figure 4.2).

Sulphate reduction profiles were monitored in parallel with sulphide depletion profiles and throughout the microcosm incubation period up to (545 h–18 days).

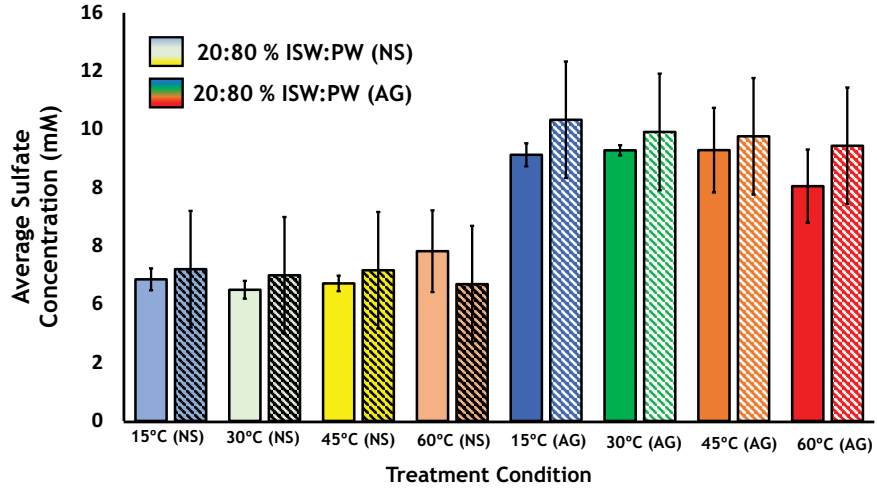

FIGURE 4.3 Effect of High Salinity PWRI Practice and temperature range (15°C–60°C) on sulphate reduction in microcosms containing 20:80% ISW: PW (NS 127 g/L TDS), and 20:80% ISW: PW (AG 204 g/L TDS). Lighter colour gradient represents average sulphate reduction (mM) for 20:80% ISW:PW (NS) treatments. Darker colour gradient represents average sulphate reduction for 20:80% ISW:PW (AG). Average sulphate concentrations (mM) were calculated for (21–161 h) timeframe (Open bars), and (329–545 h) timeframe (Shaded bars); for comparisons. Error bars represent 1 × SE. SD (NS 127 g/L) (15°C: 0.38 mM ± 0.12; 30°C: 0.74 mM ± 0.21; 45°C: 0.52 mM ± 0.15; 60°C: 0.13 mM ± 0.10;), SD (AG 204 g/L) (15°C: 0.86 mM ± 0.25; 30°C: 0.68 mM ± 0.20; 45°C: 0.65 mM ± 0.20; 60°C: 0.53 mM ± 0.15).

Sulphate reduction profiles were determined in high salinity ISW:PW and across a temperature gradient (Figure 4.3). The effect of ISW:PW (%) salinities on sulphate concentration revealed no sulphate reduction, and therefore no changes in the concentration of sulphate initially added to the microcosms (Figure 4.3). Initial concentrations of sulphate in microcosms were 4.6 mM sulphate in 20:80% ISW:PW (NS) (127 g/L TDS) incubations, and 9.8 mM sulphate in 20:80 ISW:PW (AG) (204 g/L TDS) incubations. Sulphate concentrations remained stable and close to initial microcosm concentrations by the end of the incubation period, showing no evidence of sulphate reduction across the temperature range (NS, average 4.6 ± 0.38 mM sulphate; AG, 9.8 ± 0.60 mM sulphate, Figure 4.3). No significant differences in sulphate concentrations were observed in microcosms prepared with NS or AG production waters, respectively, across the temperature range ($P = 0.32$).

4.3.2 Timeframes for Sulphide Depletion, Maximum Rate of Sulphide Depletion, and Maximum Concentration of Sulphide Depleted

To further determine the influence of the selected thermal gradient (15°C–60°C) and the high salinity PWRI mix (NS: 127 g/L TDS; AG: 204 g/L TDS), the following parameters were analysed: A) Sulphide depletion rate (mM/hrs.), B) Time to reach a sulphide depletion of 2 mM, and C) Maximum sulphide depletion concentration (mM).

4.3.2.1 Thermal Gradient Impact on Rates of Sulphide Depletion

Sulphide depletion rates in (mM/hrs.) for the salinity and temperature ISW:PW microcosms were determined (Figure 4.4). Rates of sulphide depletion (mM/hrs.) increased with the increase in the thermal gradient for (NS) the water production system (127 g/L TDS) (Figure 4.4a) but decreased with the increase in the thermal gradient for the (AG) water production system (204 g/L TDS) (Figure 4.4b). At the psychrophilic and mesophilic incubating temperatures (15°C–30°C) for the (NS) water production system, the sulphide depletion rates (mM/hrs.) were lower (0.0044 mM ± 0.00013 and 0.0045 mM ± 0.000073, respectively) compared to higher sulphide depletion observed in the lower thermophilic and moderate thermophilic incubating temperatures (45°C–60°C) for the (NS) water production system (0.0056 mM ± 0.000052 and 0.0054 mM ± 0.0002, respectively) (Figure 4.4a). In the higher salinity (AG) water production system (204 g/L TDS), the sulphide depletion rates (mM/hrs.) for the psychrophilic and mesophilic incubating temperatures (15°C–30°C) were higher (0.0044 mM ± 0.000097 and 0.0037 mM ± 0.00017) compared to the lower thermophilic and moderate thermophilic incubating temperatures (0.0029 mM ± 0.000019 and 0.0025 mM ± 0.000062, respectively) (Figure 4.4b). The sulphide depletion data (mM/hrs.) showed that at the psychrophilic incubating temperature (15°C), the sulphide depletion rates (mM/hrs.) were similar (NS: 0.0044 mM ± 0.00013; AG: 0.0044 mM ± 0.000097). However, with the increase in the thermal gradient at (30°C, 45°C, and 60°C); sulphide depletion for the (NS) water production system increased (**NS 30°C**: 0.0045 mM ± 0.000073; **NS 45°C**: 0.0056 mM ± 0.000052; **NS 60°C**: 0.0054 mM ± 0.0002) but decreased in the (AG)

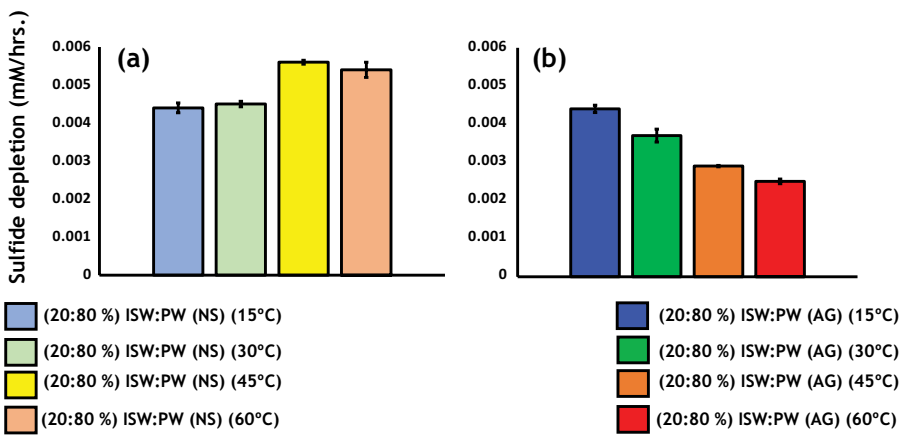

FIGURE 4.4 Sulphide depletion reaction rate (mM/hrs.) in microcosms containing the same ratios of 20% ISW – 80% PW for: (a) The North Sea water production system thermal gradient (127 g/L TDS) (15°C–60°C); (b) The Arabian Gulf (AG) water production system thermal gradient (204 g/L TDS) (15°C–60°C). Lighter colours depict reaction rates for (NS) water production system thermal gradient incubations. Darker colours depict reaction rates for (AG) water production system thermal gradient incubations. Error bars represent 1 × S.E.

water production system (**AG 30°C**: 0.0037 mM ± 0.00017; **AG 45°C: 0.0029 mM** ± 0.000019; **AG 60°C: 0.0025 mM** ± 0.000062) (Figures 4.4a, b). One-way ANOVA on Minitab was used as a statistical tool to determine the significance of the sulphide depletion rates (mM/hrs.) reported for the (NS-PW) system and the (AG-PW) system. This revealed that the differences in sulphide depletion between the (NS-PW) and the (AG-PW) system were non-significant ($P = 0.17$). However, when comparing the sulphide depletion profiles from the (NS-PW) and the (AG-PW) system with the sulphide production profile reported in 100% ISW (30°C) (no coupon incubation), the statistical tool determined the sulphide production profile significant ($P = 0.003$).

4.3.2.2 Time to Reach a Sulphide Depletion of 2mM

Time to reach a sulphide depletion of 2mM for the salinity and temperature ISW:PW microcosms were determined (Figure 4.5). Time to reach a sulphide depletion of 2mM decreased for the NS water production system thermal gradient (127 g/L TDS) (Figure 4.5a) but increased for the Arabian gulf (AG) water production system (204 g/L TDS) (Figure 4.5b). For the NS water production system thermal gradient (127 g/L TDS), the following timeframes (hrs.) to reach a sulphide depletion of 2mM were observed (**15°C**: 381 hrs.–419 hrs.; **30°C**: 427 hrs.–471 hrs.; **45°C**:313 hrs.–346 hrs.; and **60°C**: 313 hrs.–346 hrs.) (Figure 4.5a), while for the AG water production system thermal gradient (204 g/L TDS) the following timeframes (hrs.) to reach a sulphide depletion of 2mM were observed (**15°C**: 313 hrs.–346 hrs.; **30°C**: 381 hrs.–419 hrs.; **45°C**: 518 hrs.–562 hrs.; **60°C**: 518 hrs.–562 hrs.) (Figure 4.5b).

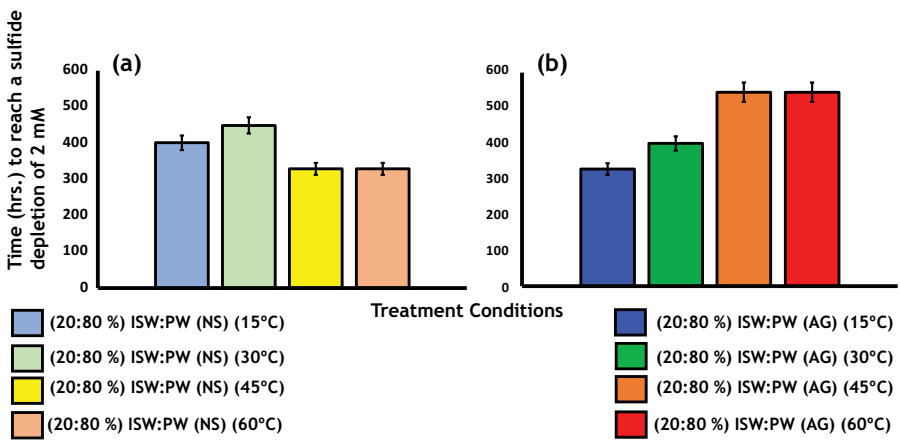

FIGURE 4.5 Time (hrs.) to reach a sulphide depletion of 2 mM across the ISW:PW ratios for: (a) The North Sea water production system thermal gradient (127 g/L TDS) (15°C–60°C); (b) The Arabian Gulf (AG) water production system thermal gradient (204 g/L TDS) (15°C–60°C). Lighter colours depict reaction rates for (NS) thermal gradient incubations. Darker colours depict reaction rates for (AG) thermal gradient incubations. Error bars represent 1 × S.E.

4.3.2.3 Maximum Sulphide Depletion

Maximum sulphide depletion (mM) for the salinity and temperature ISW:PW microcosm incubations were determined (Figure 4.6). Maximum sulphide depletion (mM) increased in the NS water production system thermal gradient incubations (Figure 4.6a) but decreased in the AG water production system thermal gradient incubations (Figure 4.6b). With increasing temperature (psychrophilic (15°C)- mesophilic (30°C)) in the (NS-PW) system, an initial slight decrease in maximum sulphide depletion from 2.64 mM ± 0.003 to 2.48 mM ± 0.08 was observed (Figure 4.6a). However, with further increases in temperature (lower thermophilic 45°C- moderate thermophilic 60°C), sulphide depletion increased (2.79 mM ± 0.007; 2.94 mM ± 0.006, respectively) (Figure 4.6a).

For the AG water production system, sulphide depletion decreased with the increase in incubating temperature (Figure 4.6b). The highest sulphide depletion was reported in the psychrophilic (15°C) (AG-PW) incubation of 2.65 mM ± 0.009 (Figure 4.6b). Lower sulphide depletion was reported in the mesophilic (30°C) (AG-PW) incubation of 2.49 mM ± 0.008 (Figure 4.6b). The lowest sulphide depletions were reported in the lower thermophilic (45°C) and moderate thermophilic (60°C) incubations (1.90 mM ± 0.005; 1.90 mM ± 0.002 respectively) (Figure 4.6b). Cross comparisons between the (NS-PW) and the (AG-PW) systems revealed that in the psychrophilic (15°C) and mesophilic (30°C) incubations, similar sulphide depletion concentrations were reported (15°C (NS-PW): 2.64 mM ± 0.003; 15°C (AG-PW): 2.65 mM ± 0.009; 30°C (NS-PW): 2.48 mM ± 0.08; 30°C (AG-PW): 2.49 mM ± 0.008) (Figures 4.6a,b). However, at the higher incubating temperatures of (lower thermophilic (45°C) and the moderate thermophilic (60°C), sulphide depletion was

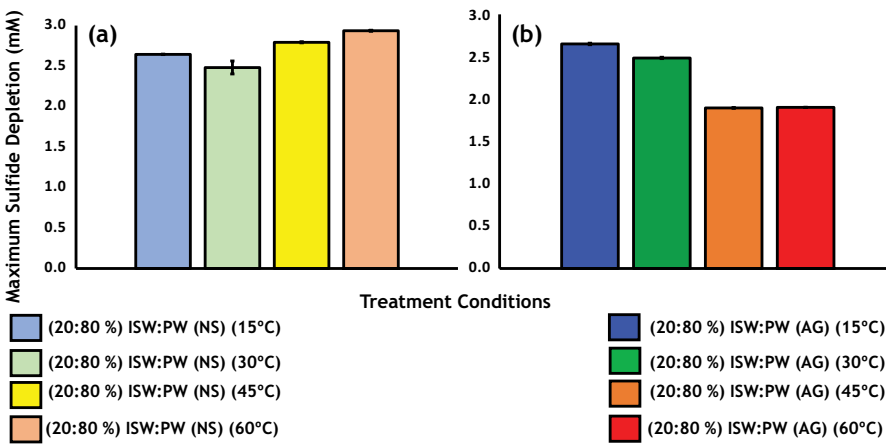

FIGURE 4.6 Maximum sulphide depletion (mM/hrs.) in microcosms containing the same ratios of 20% ISW – 80% PW for: (a) The North Sea water production system thermal gradient (127 g/L TDS) (15°C–60°C); (b) The Arabian Gulf (AG) water production system thermal gradient (204 g/L TDS) (15°C–60°C). Lighter colours depict reaction rates for (NS) thermal gradient incubations. Darker colours depict reaction rates for (AG) thermal gradient incubations. Error bars represent 1 × S.E.

higher in the (NS-PW) system incubations (45°C: 2.79 mM ± 0.007; 60°C: 2.94 mM ± 0.006) but lower in the (AG-PW) system incubations (45°C: 1.90 mM ± 0.005; 60°C: 1.90 mM ± 0.002) (Figures 4.6a,b). One-way ANOVA on Minitab was used as a statistical tool to determine the significance of the maximum sulphide depletion profiles reported for the (NS-PW) system and the (AG-PW) system. This revealed that the differences in sulphide depletion between the (NS-PW) and the (AG-PW) system were non-significant ($P = 0.21$).

4.3.3 Methanogenesis in High Salinity PWRI Practice

To determine whether other electron-accepting process than sulphate reduction was occurring under the high salinity 20:80 ISW:PW practice, methanogenesis was deemed a plausible explanation, and therefore microcosms were analysed for headspace methane production. Figure 4.7 illustrates the headspace methane production amounts in the headspace of high salinity 20:80 ISW:PW microcosms. Headspace methane in microcosms incubated at the temperature gradient of (15°C–60°C) for 20:80% ISW:PW (NS) (127 g/L TDS) and 20:80% ISW:PW (AG) (204 g/L TDS) were illustrated (Figure 4.7). Based on the stoichiometric conversions of VFAs to methane, mmoles amounts of methane should be produced from the mmoles amounts of VFAs oxidised (Equations 4.7–4.8). For example, 1mmole acetate oxidation will be coupled to 1 mmole methane (CH_4) reduction by the activity of acetoclastic methanogens (Equation 4.8), and 1mmole reduction of CO_2 by 1mmole H_2; as a result, for the activity of hydrogenotrophic methanogens (Equation 4.7). However, the actual masses of methane detected in the headspace of microcosms, however, were 6 orders of magnitude lower than the envisioned VFA to methane stoichiometry (6.50 nmoles CH_4 ± 0.07; range 6.11–8.02 nmoles CH_4; Figure 4.7), ruling out the possibility for methanogenesis being a potential electron-accepting process under such high salinity ISW:PW systems.

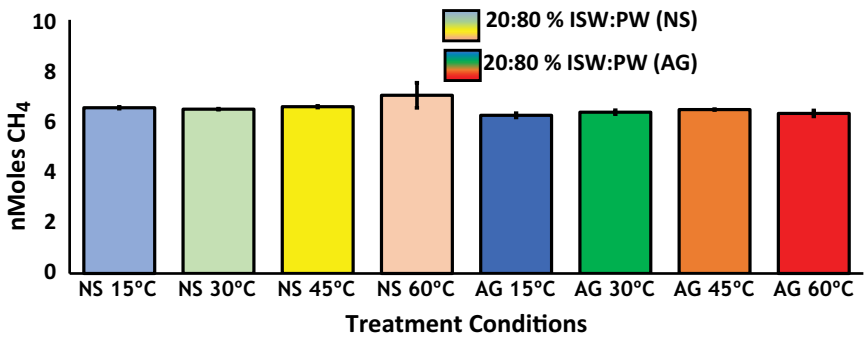

FIGURE 4.7 Mass of methane (nMoles) detected in headspace of anoxic microcosms containing 20:80% ISW: PW (NS) (127 g/L TDS), and 20:80% ISW: PW (AG) (204 g/L TDS). Lighter colour gradient represents headspace methane in 20:80% ISW:PW (NS) (127 g/L TDS) microcosmos. Darker colour gradient represents headspace methane in 20:80% ISW:PW (AG) (204 g/L TDS) microcosms. Error bars represent 1 × SE.

4.3.4 Gravimetric Analyses, Surface Morphology, and Surface Elemental Composition of Corrosion Coupons

Corrosion rates in millimetres per year (mm/yr.) from the high salinity 20:80 ISW:PW practice microcosms were calculated and displayed (Figure 4.8a,b). Overall corrosion rates from both the ISW:PW (NS) and ISW:PW (AG) were low <0.02 mm/yr. (Figure 4.8a,b). However, corrosion rates were slightly increased at 30°C (0.011 ± 0.0002 mm/yr.; Figure 4.8a) and 60°C (0.018 ± 0.0004; Figure 4.8a) in the NS ISW:PW system, compared to other treatments of NS and AG-PW corrosion coupon samples. (NS: 0.002 ± 0.0003 mm/yr. 15°C; NS: 0.003 ± 0.0006 mm/yr. 45°C) (Figure 4.8a) (AG: 0.002 ± 0.0008 mm/yr. 15°C; 0.002 ± 0.0004 mm/yr. 30°C; 0.003 ± 0.0005 mm/yr. 45°C, and 0.002 ± 0.0002 mm/yr. 60°C (Figure 4.8b).

Selected corrosion coupons (Figure 4.8a stars) were further inspected for surface morphology and elemental composition, using SEM-EDS, to corroborate results of the gravimetric analyses, in comparison to controls. Figures 4.9 and 4.10 illustrate the surface morphology of the corrosion coupons. Corrosion coupon surface morphology for the selected 20:80% (ISW: PW) (NS) (127 g/L TDS) coupon samples highlighted in Figure 4.8 are displayed in Figures 4.9 and 4.10. Surface morphology of coupon surfaces of 20:80% (ISW: PW) (NS) incubated at 30°C and 60°C revealed the development of advanced-stage pitting nucleations (0.17–0.22 pits of 20 μm, and 1400 pits of 50 μm–150 μm, for pits number and diameter per cm^2, respectively for 30°C and 60°C incubations; Figure 4.9). By comparison, the control coupon (chemically treated with HCl, and NaOH, removing the corrosion inhibitor film – no incubation) exhibited a flat and uniform surface morphology and showed no evidence of pitting nucleations (Figure 4.9). Morphological variations in the pits were observed under 20:80% (ISW: PW) at 30°C coupon (wide-shallow pitting nucleation (Figure 4.9); sub-surface pitting nucleation (Figure 4.10). Nano-characterisation of

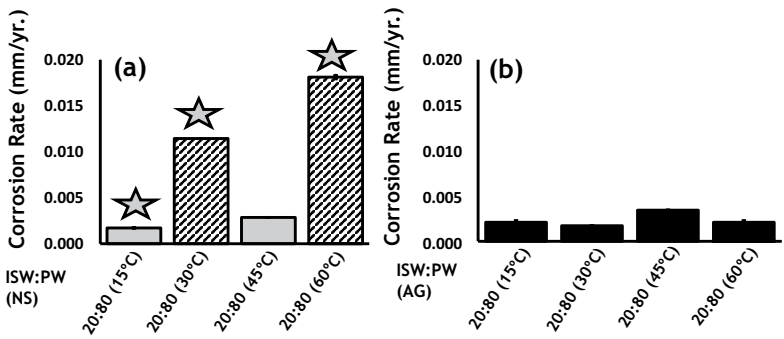

FIGURE 4.8 Corrosion Rates in (mm/yr.) for: (a) The North Sea water production system (127 g/L TDS) temperature gradient incubations (15°C–60°C) (Gray filled bars); and (b) The Arabian Gulf water production system (204 g/L TDS) temperature gradient incubations (15°C–60°C) (Black filled bars). Diagonally striped bars represent ISW:PW incubations with highest corrosion rates (mm/yr.) Selected samples (star) were subjected to SEM/EDS analyses. Error bars represent 1 × S.E.

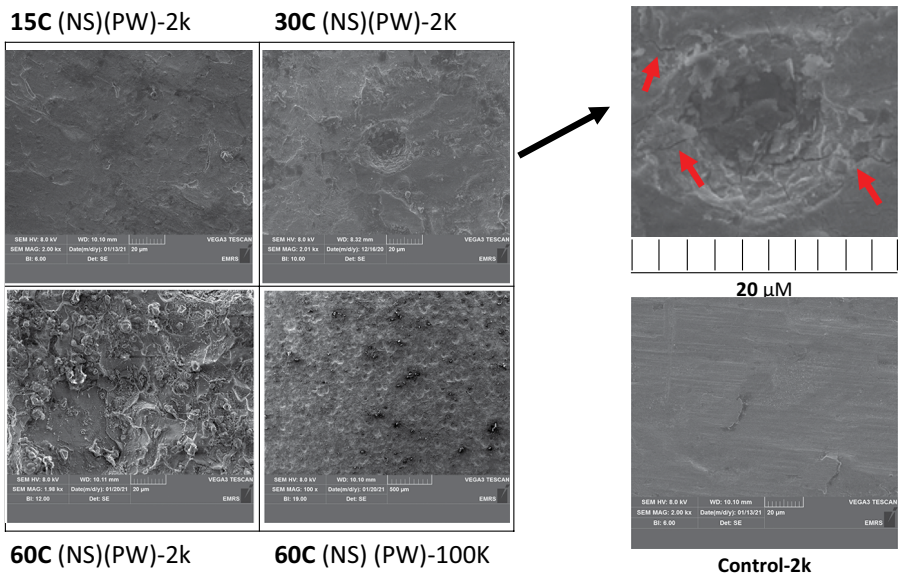

FIGURE 4.9 Scanning Electron Microscopy (SEM) images from steel coupons incubated in anoxic microcosms of 20:80% (ISW: PW) (NS) (127 g/L TDS) at 15°C, and 30°C (2K magnification), 60°C (2K and 100K magnifications), and control coupon (2K and 100K magnifications). Red arrows indicate detected cracks within the wide-shallow pitting nucleation and on coupon surface.

the elemental composition for the pitted surfaces was performed on corrosion coupons of (20:80%) ISW: PW (NS) (30°C) and (20:80%) ISW: PW (NS) (60°C). Table 4.2 illustrate EDS elemental composition of corrosion coupon surface.

Energy Dispersive Spectroscopy of corrosion coupon surface is displayed in Table 4.2. Seven different elements were detected on the coupon surface: carbon, oxygen, sodium, phosphorus, potassium, calcium, and iron. Three elements dominated the atomic composition (%) of pitted surfaces at both 30°C and 60°C incubations – oxygen (30°C Min. 42.41%; Max. 49.61%, 60°C Min. 43.37%; Max. 59.15%), carbon (30°C Min. 9.83%; Max. 41.27% 60°C Min. 11.47%, Max. 39.01%), and finally iron (30°C Min. 7.70%; Max. 32.09%, 60°C Min. 8.48%, Max. 19.28%) (Table 4.2). Iron oxides were envisioned to be one of the main deposits present under both the 30°C and 60°C incubations (20:80%) ISW:PW (NS) coupons. This was evident in the concurrence of the abundant elemental compositions (%) of both iron and oxygen elements, suggesting the corrosion susceptibility of these environments. Furthermore, under both the 30°C and 60°C incubations (20:80%) ISW:PW (NS) coupons, strong evidence for the presence of both phosphate and carbonate deposits was observed. This was reported by looking at the ionic (%) contributions of carbon, oxygen, and phosphorus elements to these respective deposits (i.e., phosphates and carbonates) (1 carbon: 3 oxygen) for carbonates; (1 phosphorus: 4 oxygen) for phosphates (Table 4.2).

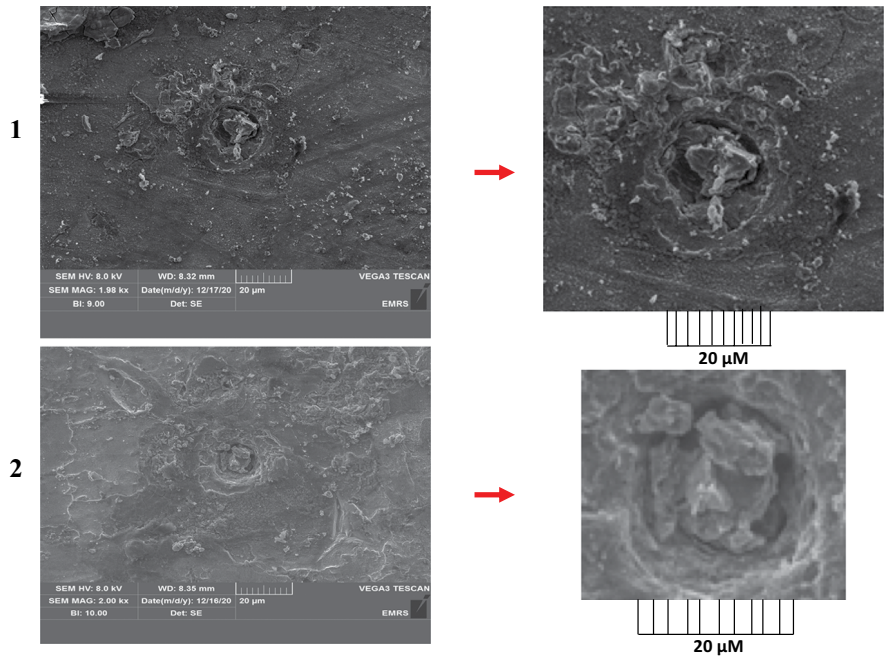

FIGURE 4.10 Other pitting nucleations on steel coupons incubated in anoxic microcosms of 20:80% (ISW: PW) (NS) at 30°C (2K magnification). Red arrows show the zoomed-in view and the morphological characterisation of nucleation (sub-surface nucleation).

TABLE 4.2
Energy Dispersive Spectroscopy (EDS) Elemental Compositions of Corrosion Coupon Surfaces from Anoxic Microcosms 20:80% (ISW: PW) (NS) (30°C) and 20:80% (ISW: PW) (NS) (60°C)

Element	Atomic Composition (%)					
	(20:80%) ISW:PW (NS)-30°C			(20:80%) ISW:PW (NS)-60°C		
	Coupon 1	Coupon 2	Coupon 3	Coupon 1	Coupon 2	Coupon 3
Carbon	13.77	41.27	9.83	11.47	17.74	39.01
Oxygen	45.50	42.41	49.61	59.15	54.02	43.37
Sodium	4.74	1.36	3.11	6.66	3.24	1.48
Phosphorus	11.79	4.91	4.62	7.92	4.27	4.77
Potassium	1.58	N.D.	0.75	0.85	0.44	0.74
Calcium	1.24	2.34	N.D.	0.39	1.01	2.15
Iron	21.35	7.70	32.09	13.56	19.28	8.48
SUM	100	100	100	100	100	100

N.D. Non-detected.

4.3.5 Microbial Community Analysis

The microbial communities selected under the different conditions of thermal gradient (15°C–60°C), and the high salinity ISW:PW mix of 20:80 ISW:PW (NS) (127 g/L TDS), and the 20:80 ISW:PW (AG) (204 g/L TDS) were analysed by *16S rRNA* gene-based analysis.

Principal Component Analysis of species level *16S rRNA* gene profiles of microbial communities from anoxic microcosms containing the eight different treatment conditions (with corrosion coupons) in Table 4.1 and representing the (NS) and the (AG) PW system (15°C–60°C) was conducted. The analysis was conducted on the basis of Bray-Curtis similarities of the species level *16S rRNA* gene profiles.

4.3.5.1 Overview of Microbial Community Dynamics for Thermal Gradient (15°C–60°C) Incubations at Different Salinities

Principal Component Analysis of *16S rRNA* gene profiles for microbial community dynamics for the thermal gradient (15°C–60°C), for the 20:80% (ISW:PW) (NS) (127 g/L TDS), and the 20:80% (ISW:PW) (AG) (204 g/L TDS) incubations are illustrated in Figure 4.11. PCA revealed distinct clusters according to temperature (Figure 4.11). Whereby communities from the 20:80% ISW:PW (NS) and the 20:80% ISW:PW (AG) microcosms incubated at the lower temperatures of 15°C and 30°C clustered together, and communities incubated at 20:80% ISW:PW (NS), and 20:80% ISW:PW (AG), higher temperatures of 45°C and 60°C formed a separate cluster (high-temperature cluster), together with River Tyne sediment microbial

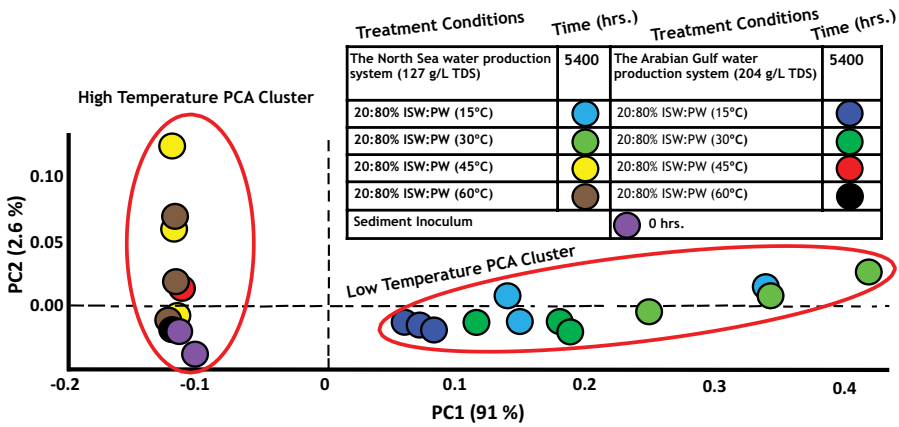

FIGURE 4.11 Principal Component Analysis (PCA) of *16S rRNA* gene profiles from microbial communities in anoxic microcosms at the end of incubations (5400 hrs.–225 days) in ISW: PW incubations of 20:80 ISW:PW from the North Sea water production system (127 g/L TDS), and the Arabian Gulf water production system (204 g/L TDS), incubated at a thermal gradient of (15°C–60°C). End of incubations (5400 hrs.–225 days) (ISW:PW) PCA clusters were compared against the time (0 hrs.–0 days) of sediment inoculum preserved at –20°C prior to utilisation in *16S rRNA* gene profiling analyses. Principal components PC1 and PC2 explained 91.0% and 2.6% of the variance, respectively.

inoculum (Figure 4.11). The first principal component explained 91% of the variation in the dataset (PC1), with 2.6% variation explained on the second principal component dimension (PC2) (Figure 4.11).

Next, heatmaps were generated, to display the relative abundance (%), based on the top 10 most abundant microbial phyla/orders identified across 20:80% ISW:PW (NS), and 20:80% ISW:PW (AG) thermal gradient incubations (15–60°C). Relative abundances (%) for ISW:PW systems were based on end of incubations (5400 hrs.–225 days) samples, compared against the sediment inoculum (0 hrs.–0 days) samples. Figures 4.12 and 4.13 illustrated the generated 20:80% ISW:PW (NS) and 20:80% ISW:PW (AG) heatmaps, respectively.

Low-temperature incubations (15°C and 30°C) appeared to drive the selective enrichment of bacteria from the order *Halanaerobiales* in both the (NS) and (AG) PW systems (Figures 4.12 and 4.13, respectively) – ~35% relative abundance for NS 15°C replicates 1–3, and ~ 50% relative abundance for NS 30°C replicates 1–3 (Figure 4.12). For the Arabian gulf samples however, lower *Halanaerobiales* relative abundance was reported in AG 15°C replicates 1–3 (~ 20% relative abundance), and in AG 30°C replicates 1–3 (~30% relative abundance) (Figure 4.13). By comparison, microcosms at the higher temperatures (45°C, and 60°C) were dominated by the

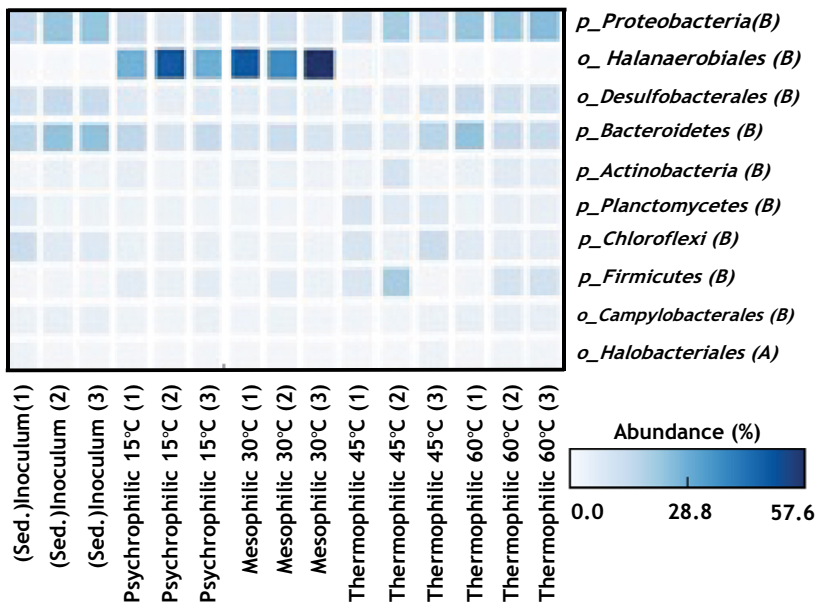

FIGURE 4.12 Heatmap representing the Top 10 bacterial phyla/orders (vertical-axis) detected in (20:80%) ISW:PW (NS) (127 g/L TDS) thermal gradient incubation microcosms (15°C–60°C). Relative abundances are indicated by colour intensity with darker blue shades depicting higher relative abundance and lighter shades depicting lower relative abundance. All end of incubation (5400 hrs.–225 days) ISW:PW microcosms were compared against the Sediment inoculum (0 hrs.) samples. Data from three replicate samples per thermal gradient are shown and the samples were re-ordered based upon increasing order of the thermal gradient (15°C–60°C).

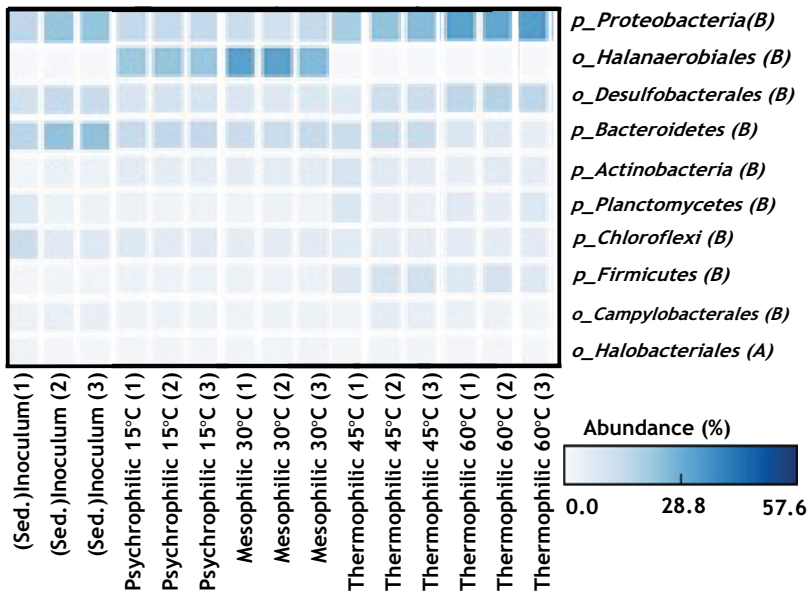

FIGURE 4.13 Heatmap representing the top 10 bacterial phyla/orders (vertical-axis) detected in microcosms containing (20:80%) ISW:PW (AG) (204 g/L TDS) thermal gradient incubation microcosms (15°C–60°C). Relative abundances are indicated by colour intensity with darker blue shades depicting higher relative abundance and lighter shades depicting lower relative abundance. All end-of-incubation (5400 hrs.–225 days) ISW:PW microcosms were compared against the sediment inoculum (0 hrs.) samples. Data from three replicate samples per thermal gradient are shown, and the samples were re-ordered based upon increasing order of the thermal gradient (15°C–60°C).

microbial phyla/orders of *Proteobacteria, Desulfobacterales and Bacteroidetes*, which accounted for ≥10% relative abundance in total in both (20:80%) ISW:PW (NS) and (20:80%) ISW:PW (AG) incubations, and similar to the phylum/order microbial enrichments detected in River Tyne sediment inoculum control (Figures 4.12 and 4.13, respectively).

The species diversity in all thermal gradient (15°C–60°C) incubated microcosms were compared using the Shannon indices based upon the (5400 hrs.) datapoint for ISW:PW incubations, and the (0 hrs.) datapoint for the sediment inoculum (Figures 4.12 and 4.13 respectively). Shannon indices for microbial communities selected at the thermal gradient (15°C–60°C) for (20:80%) ISW:PW (NS) incubations were: psychrophilic incubation (15°C): 7.22 ± 0.55; mesophilic incubation (30°C): 6.77 ± 0.43; lower thermophilic incubation (45°C): 8.52 ± 0.52; and moderate thermophilic incubation (60°C): 8.71 ± 0.69 (Figure 4.12). In comparison to the NS water production system (Figure 4.12), the AG water production system (Figure 4.13) exhibited a similar Shannon indices profile (i.e., lower Shannon indices values for lower temperature incubations (15°C–30°C); and higher Shannon indices values for the higher temperature incubations (45°C–60°C), and were: psychrophilic incubation (15°C): 7.50 ± 0.50; moderate incubation (30°C): 6.71 ± 0.64; lower thermophilic incubation

(45°C): 8.98 ± 0.65; and moderate thermophilic incubation (60°C): 8.96 ± 0.63 (Figure 4.13). For sediment inoculum controls, the Shannon indices were very similar (8.85 ± 0.13), compared to the lower and moderate thermophilic incubations (45°C incubation average: 8.75 ± 0.59; 60°C incubation average: 8.84 ± 0.66) ($P \geq 0.05$), but quite different (8.85 ± 0.13), compared to the low-temperature incubations (15°C incubation average: 7.36 ± 0.53; 30°C incubation average: 6.74 ± 0.54 selective enrichments ($P \leq 0.05$).

Therefore, based on the Shannon indices, higher microbial diversity, and much lower relative abundance (≥10%) for both the high-temperature microbial inoculum (45°C, and 60°C incubations) and River Tyne sediment inoculum control were observed (Figures 4.12 and 4.13 respectively). Additionally, lower microbial diversity and much higher relative abundance (20%–50%) for low-temperature microbial inoculum (15°C–30°C) compared to the sediment inoculum were observed (Figures 4.12 and 4.13, respectively).

4.3.5.2 Detailed Analysis of Microbial Community Dynamics for River Tyne Sediment Inoculum

An illustration of the microbial diversity for River Tyne Sediment inoculum is displayed in (Figure 4.14). The relative abundance (%) of the top 12 species/genera detected ranged from 1 to just over 7% (Figure 4.14). Ten of these taxa were present at relative abundances of (1%–2%) and with a greater relative abundance of two *Woeseia* sp. that had a relative abundance of 7.1 ± 1.16% and 6.6 ± 1.12%, respectively (Figure 4.14).

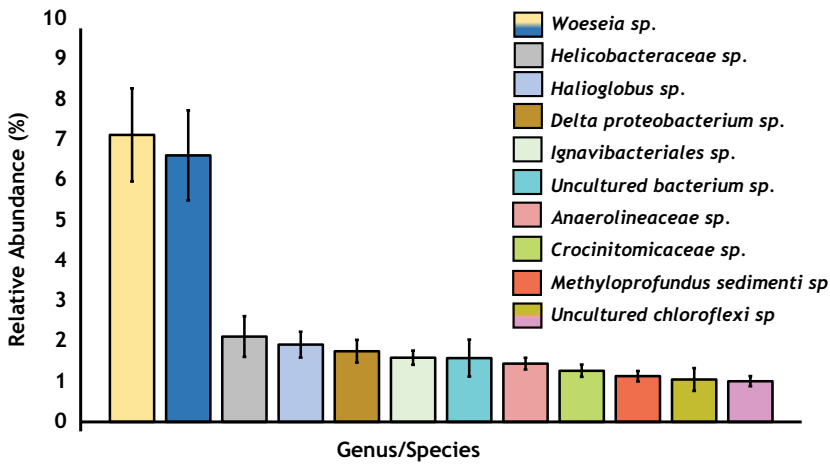

FIGURE 4.14 *16S rRNA* gene copy number adjusted relative abundance (%) at species/genus level for River Tyne Sediments Microbial Inoculum. An illustration for the diversity of microbial genera of *Woeseia* sp. denoted with yellow/blue coloured bars, and the other microbial genera denoted with different coloured bars. Sediment inoculum microbial diversity was based on (0 hrs.) samples preserved at −20°C prior to *16S rRNA* gene profiling analyses. Error bars represent 1 × S.E.

4.3.5.3 Detailed Analysis of Microbial Community Dynamics for the North Sea Water Production System Thermal Gradient (15°C–60°C)

A comparative illustration of the microbial diversity of the enriched *Halanaerobium* sp. across the NS water production, and the AG water production system (Figure 4.15), and other microbial species enrichments for the NS water production system's thermal gradient (15°C–60°C) (Figure 4.16) are displayed. A significant enrichment in relative abundance of the genus *Halanaerobium* was observed under the NS water production system: 20:80 15°C: two different *Halanaerobium* species were enriched at 22.58 ± 1.23% and 11.96 ± 1.74%, respectively, 20:80 30°C: two different *Halanaerobium* species were enriched at 31.02 ± 2.34%, and 13.6 ± 1.87%, respectively (Figure 4.15a), and the AG water production system: 20:80 15°C: only one *Halanaerobium* sp. enriched at 20.66 ± 0.93%, and for 20:80 30°C: three different *Halanaerobium* species were enriched at 24.3± 1.62%, 3.07 ± 0.46%, and 1.13 ± 0.01% respectively (Figure 4.15b). However, *Halanaerobium* sp. sequences were not detected in the lower thermophilic (45°C) and the moderate thermophilic (60°C) incubations from both the NS water production and the AG water production systems (Figure 4.15a,b). No SRP enrichments were observed under the NS water production system (NS) (127 g/L TDS) or the AG water production system (204 g/L TDS) incubations (Figure 4.15a,b, respectively).

In contrast, from the microcosm experiments conducted by Sindi, *et al*. (2021), and under 100% ISW (42 g/L TDS) salinity, the microbial enrichment results

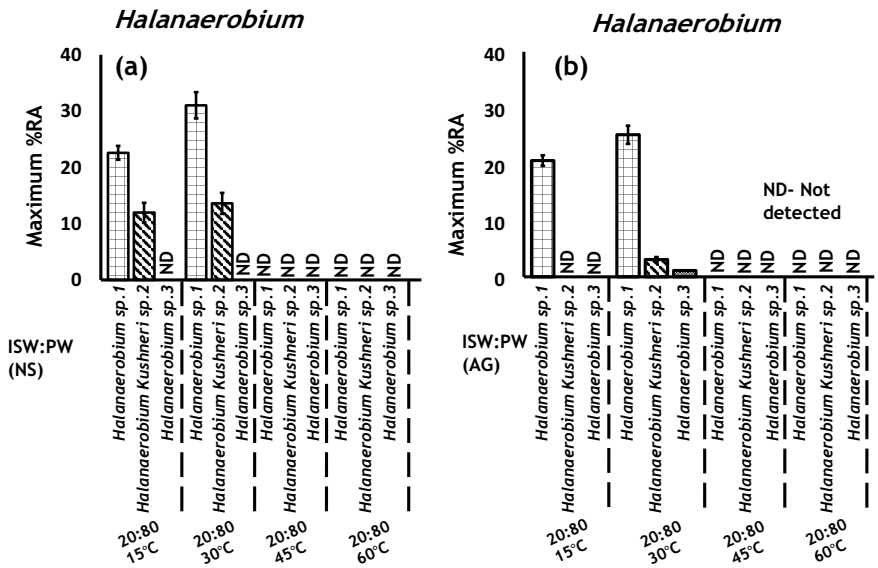

FIGURE 4.15 *16S rRNA* gene copy number adjusted relative abundance (%) at species/genus level for ISW:PW incubations from the North Sea (NS) and the Arabian Gulf (AG) water production systems. A comparative illustration of the diversity of the enriched *Halanaerobium* sp. for: (a) The North Sea water production system (NS) and (b) The Arabian Gulf water production system. Error bars represent 1 × SE.

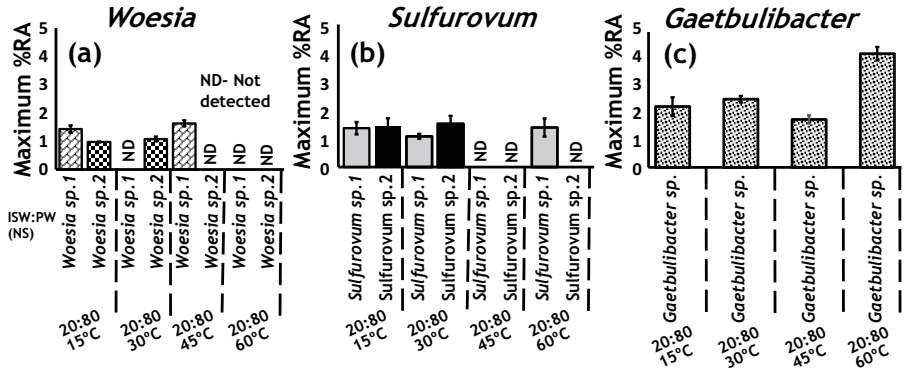

FIGURE 4.16 *16S rRNA* gene copy number adjusted relative abundance (%) at species/genus level for ISW:PW incubations from the North Sea (NS) water production system. An illustration of the diversity of the other enriched or detected species of: (a) *Woesia* sp., (b) *Sulfurovum* sp., and (c) *Gaetbulibacter* sp. Error bars represent 1 × SE.

revealed a significant (Maximum) enrichment of the SRP microbial consortium of *Desulfobulbus* sp., *Desulfobacter* sp., and *Desulfotignum* sp. between (31–75 days) post-incubation (*Desulfobulbus* sp.: 18.62 ± 2.30% at 55 days post-incubation; *Desulfotignum* sp.: 4.33 ± 0.49% at 55 days post-incubation; and *Desulfobacter* sp.: 8.40 ± 1.40% at 55 days post-incubation (Sindi, *et al*., 2021). Therefore, this experiment revealed that elevated salinities under (30°C) incubations inhibited sulphate reduction, therefore, inhibiting the enrichment of sulphate-reducing microorganisms.

High-temperature incubations (45°C–60°C) coupled with high salinity (i.e., 127 g/L TDS ISW:PW (NS) resulted in no microbial community changes, whereby the microbial communities under the high-temperature incubations (45°C–60°C), and under the NS water production system, were detected at relative abundance (%) of between 1–2% (except for *Gaetbulibacter* sp.) and looked like those of the River Tyne microbial inoculum controls (Figure 4.16a–c). Additionally, no sulphate-reducing microorganisms were enriched under 20:80 45°C and 20:80 60°C incubations (Figure 4.16a–c).

In both the low- and high-temperature microbial enrichments (15°C–60°C), *Woeseia* sp., *Sulfurovum* sp., *and Gaetbulibacter* sp. were consistently detected as the most abundant taxa (Figure 4.16) (*Woesia* sp.: two different species were detected, and maximum %RA of 1.63 ± 0.11 detected at 225 days post-incubation; *Sulfurovum* sp., two different species were detected and maximum %RA 1.52 ± 0.28 detected at 225 days post-incubation; and one *Gaetbulibacter* sp. detected with a maximum %RA of 4.20 ± 0.25 detected at 225 days post-incubation (Figure 4.16a–c)). The prevalence of *Woesia* sp. as more abundant in the sediment control (7.1 ± 1.16% and 6.6 ± 1.12% (Figure 4.14)), compared to the high-temperature incubations point towards the high-temperature systems (i.e., 45°C and 60°C incubations) not showing much microbial activity and therefore the high temperature (45°C–60°C) treatments not eliciting a major population shift (Figure 4.16a–c).

4.3.5.4 Detailed Analysis of Microbial Community Dynamics for the Arabian Gulf Water Production System Thermal Gradient (15°C–60°C)

A comparative illustration of the microbial diversity of the enriched *Halanaerobium* sp. across the NS water production and the AG water production system is displayed in Figure 4.15a,b, and other microbial species enrichments for the AG water production system's thermal gradient (15°C–60°C) are displayed in Figure 4.17.

A comparative illustration for the diversity of the enriched *Halanaerobium* sp. across the NS water production system and the AG water production system is displayed (Figure 4.15a,b). As elicited, the diversity of the enriched *Halanaerobium* sp. was greater for the AG water production system 20:80 30°C incubations but with much lower relative abundance (%) for *Halanaerobium Kushneri sp.2* and *Halanaerobium sp.3* (3.07 ± 0.46%, and 1.13 ± 0.01%, respectively (Figure 4.15b) compared to the 20:80 30°C incubation for the NS water production system (13.6 ± 1.87% and sequences not detected for *Halanaerobium sp.3*, respectively) (Figure 4.15a).

Similar to the NS water production system, high temperature coupled with high salinity (i.e., 204 g/L TDS ISW:PW (AG) resulted in no microbial community changes, whereby the microbial communities under the high-temperature incubations (45°C–60°C) were detected at relative abundance (%) of between 1% and 2% (except for *Sulfurovum* sp. and *Gaetbulibacter* sp.) and looked like those of the River Tyne microbial inoculum controls (Figure 4.17a–c). Additionally, no sulphate-reducing microorganisms were enriched under 20:80 45°C and 20:80 60°C incubations (Figure 4.17a–c).

In both the low- and high-temperature microbial enrichments (15°C–60°C), *Woeseia* sp., *Sulfurovum* sp., *and Gaetbulibacter* sp. were consistently detected as the most abundant taxa (Figure 4.17) (*Woesia* sp.: two different species were detected, and maximum %RA of 2.06 ± 0.23 detected at 225 days post-incubation; *Sulfurovum*

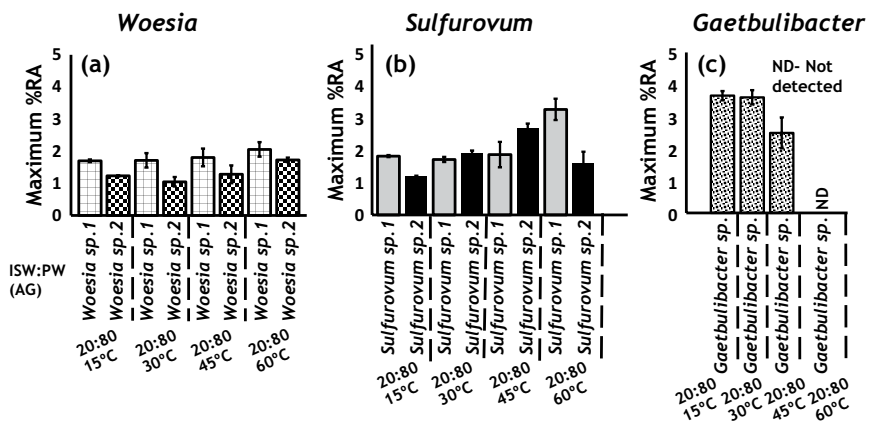

FIGURE 4.17 *16S rRNA* gene copy number adjusted relative abundance (%) at species/genus level for ISW:PW incubations from the Arabian Gulf (AG) water production system. An illustration of the diversity of the other enriched or detected species of: (a) *Woesia* sp., (b) *Sulfurovum* sp., and (c) *Gaetbulibacter* sp. Error bars represent 1 × SE.

sp., two different species were detected and maximum %RA 3.10 ± 0.31 detected at 225 days post-incubation; and one *Gaetbulibacter* sp. detected with a maximum %RA of 3.65 ± 0.15 detected at 225 days post-incubation (Figure 4.17a–c)). The prevalence of *Woesia* sp. as more abundant in the sediment control (7.1 ± 1.16% and 6.6 ± 1.12% (Figure 4.14) compared to the high-temperature incubations point towards the high-temperature systems (i.e., 45°C and 60°C incubations) not showing much microbial activity and the treatment not eliciting a major population shift (Figure 4.16a–c).

4.4 DISCUSSION

4.4.1 Trends in Microbial Communities Coupled with Electron Acceptor to VFA Stoichiometry

The process of sulphate reduction follows the notion of sulphate reduction (electron acceptor), leading to H_2S production (Kaksonen and Puhakka, 2007; (Lens, *et al.*, 2002). Typically, under sulphate-reducing environments, the longer chain VFAs (i.e., butyrate and propionate) are oxidised to acetate coupled to sulphate reduction. 1 mole of butyrate is oxidised to 2 moles of acetate coupled to the reduction of 0.5 moles of sulphate into sulphide (Equation 4.1). Similarly, 1 mole of propionate is converted to 1 mole of acetate at the expense of 0.75 moles of sulphate reduced into sulphide (Equation 4.2). Acetate is oxidised completely to CO_2 with a 1:1 stoichiometry of acetate to sulphate – reduced to sulphide (Equation 4.3). Equations 4.1–4.3 illustrate the VFAs oxidation coupled to sulphate reduction equations utilised by the enriched anaerobic SRP communities:

$$2C_4H_7O_2^- + SO_4^{-2} \rightarrow 4C_2H_3O_2^- + HS^- + H^+ \quad (4.1)$$

(Chen, *et al.*, 2017)

$$4C_3H_5O_2^- + 3SO_4^{-2} + 3H^+ \rightarrow 4C_2H_3O_2^- + 3HS^- + 4CO_2 + 4H_2O \quad (4.2)$$

(Chen, *et al.*, 2017)

$$C_2H_3O_2^- + SO_4^{-2} + \rightarrow 2HCO_3 + HS^- \quad (4.3)$$

(Widdel and Bak, 1992)

Stoichiometric conversions of VFAs coupled to sulphate reduction was displayed (Equations 4.1–4.3). Based on VFAs additions to the NS water production incubations, and the AG water production incubations, it was envisioned that the enriched microbial communities utilised VFAs as the electron donors. Sulphate reduction results revealed no significant sulphate reduction occurring across the NS water production system or the AG water production system from the baseline sulphate (mM) concentrations of (NS ≈ 5 mM; AG ≈ 10 mM) (Table 4.1) ((NS, average 4.6 ± 0.38 mM sulphate; AG, 9.8 ± 0.60 mM sulphate) measured between day 1 and day 22 post-incubation (Figure 4.3). Therefore, it was envisioned that potentially another electron-accepting process such as hydrogenotrophic or acetoclastic methanogenesis (i.e., utilising H^+ protons or acetate respectively) as potential electron-accepting

processes could have been at play under the NS and the AG water production system. Methanogens were reported to utilise VFAs (acetate, butyrate, and propionate) as electron donors to produce headspace methane (Blake, *et al*., 2020; Tian, *et al*., 2019). Equations 4.4–4.8 illustrate the chemical reactions in the four steps of anaerobic digestion (AD) of hydrolysis, acidogenesis, acetogenesis, methanogenesis, and highlighting the hydrogenotrophic methanogens activity (utilising H^+ protons as electron acceptors) and the acetoclastic methanogens activity (utilising acetate as electron acceptors):

$$C_3H_5O_2^- + 3H_2OC_2H_3O_2^- + HCO_3^- + H^+ + 3H_2\Delta G^{0/} = +76.0 \text{ KJ mol}^{-1} \quad (4.4)$$

(Tian, *et al*., 2019)

$$C_4H_7O_2^- + 2H_2O2C_2H_3O_2^- + H^+ + 2H_2 + \Delta G^{0/} = +48.0 \text{ KJ mol}^{-1} \quad (4.5)$$

(Tian, *et al*., 2019)

$$C_2H_3O_2^- + 4H_2O_2HCO_3^- + 4H_2 + H^+ \Delta G^{0/} = +104.6 \text{ KJ mol}^{-1} \quad (4.6)$$

(Tian, *et al*., 2019)

$$HCO_3^- + 4H_2 + H^+ CH_4 + 3H_2O \Delta G^{0/} = -135.6 \text{ KJ mol}^{-1} \quad (4.7)$$

(Tian, *et al*., 2019)

$$C_2H_3O_2^- + H_2OCH_4 + HCO_3^- \Delta G^{0/} = -31.0 \text{ KJ mol}^{-1} \quad (4.8)$$

(Tian, *et al*., 2019)

Anaerobic digestion (AD) of VFAs is usually mediated by four steps: hydrolysis, acidogenesis, acetogenesis, and methanogenesis (Angelidaki, *et al*., 2011). The complex VFA polymers (e.g., propionate and butyrate) are initially hydrolysed into the VFA monomer (acetate) during hydrolysis (Equations 4.4–4.5) (Tian, *et al*., 2019), and consequently converted into acetate during acetogenesis (Equations 4.4–4.6). The released electrons from VFA polymers (propionate and butyrate) are then channelled into H^+ generating hydrogen protons (Equations 4.4–4.5). Although the hydrolysis of propionate and butyrate into acetate generating H^+ is thermodynamically unfavourable, this process would not proceed unless coupled with hydrogenotrophic methanogenesis to consume the generated H^+ protons (Tian, *et al*., 2019). Finally, for methane to be produced, one of two pathways must be followed: A) oxidation of acetate coupled to methane production (Equation 4.8) or B) reduction of CO_2 by H_2 (Equation 4.7).

From this ISW:PW experimental incubations methanogenesis occurrence as a potential terminal electron accepting process was evaluated under the NS water production system (127 g/L TDS) and the AG water production system (204 g/L TDS) incubations (Table 4.1). Headspace methane measured, however, were in nmoles amounts compared to the envisioned (1:1) ratio for acetate oxidation coupled to methane production by acetoclastic methanogens (Equation 4.7), or the (1:1) ratio of propionate and butyrate oxidation into H^+ protons by hydrolysis for the hydrogenotrophic methanogens then to feed on the generated H^+ (Equations 4.4–4.5). Therefore,

for hydrogenotrophic methanogenesis to have been at play consuming the VFAs mixture added to these (NS) and (AG) ISW:PW incubations, 10 mmoles H^+ (from 10 mmoles propionate hydrolysis) (Equation 4.4) and 5 mmoles H^+ (from 5 mmoles butyrate hydrolysis) (Equation 4.5) must have been produced in the headspace of ISW:PW microcosms. However, the previous statement was not supported with the NGS datasets whereby at the end incubations (225 days–5400 hrs.) acetolactic methanogens or hydrogenotrophic methanogens *16S rRNA* gene sequences were not detected (Figures 4.12 and 4.13), and headspace methane in ISW:PW incubations representing the (NS) production water system (127 g/L TDS) and the AG water production system (204 g/L TDS) were seven to nine orders of magnitude lower (in Figure 4.7) than the stoichiometric conversions of VFAs-methane (Equations 4.4–4.8). Compared to the follow-up experiment run with ISW (NS) (42 g/L TDS) incubations, the acetoclastic methanogenic archaeal family of *Methanosaeta 16S rRNA* gene sequences were detected at the end of incubations (225 days–5400 hrs.) (Sindi, *et al*., 2021).

The microbial community analysis revealed a strong selection of *Halanaerobium* sp. (Figure 4.15) implicated in Guar Gum degradation during drilling and hydraulic fracturing workover procedures (Booker, *et al*., 2017), and with the reported *Halanaerobium* sp. to utilise thiosulfate/elemental sulphur (i.e., electron acceptors) coupled to VFA metabolism (i.e., mainly acetate) (Booker, *et al*., 2017). It was hypothesised that the dominant *Halanaerobium* sp. in the fractured shale formation decomposed of Guar gum and produced acetate and sulphide as by-products from the polysaccharide (Guar gum) degradation (Liang, *et al*., 2016; Lipus, *et al*., 2017).

However, since thiosulfate ($S_2O_3^-$) or elemental sulphur (S^0) were not added and therefore not measured in the ISW:PW incubations, it would not be possible to quantify the use of these as electron acceptors by the enriched *Halanaerobium* sp., which leads the way to the only other possibility of fermentative metabolism of carbohydrates being the most plausible explanation for the observed enrichments of *Halanaerobium* sp. in this ISW:PW experiment, and consistent with earlier literature (Abdeljabbar, *et al*., 2013; Booker, *et al*., 2017, 2019; Kögler, *et al*., 2021; Lipus, *et al*., 2017).

Systematic, sulphide depletion profiles observed in both the NS water production system (NS) (127 g/L TDS) and the AG water production system (204 g/L TDS) (Figure 4.1) illustrated that the added oxygen scavenger ($Na_2S.9H_2O$) (5 mM) was rapidly removed from the ISW:PW systems (NS average sulphide depletion: 2.63 ± 0.23 (Figure 4.6a); AG average sulphide depletion: 2.15 ± 0.32) (Figure 4.6b), possibly suggesting the transformation of the depleted sulphide into iron sulphide (FeS) biotically or abiotically. Equations 4.9–4.10 illustrate the SRP cathodic depolarisation procedure by SRP to produce iron sulphide (FeS) black films on coupon surface, and the consequent mineralisation of the produced (FeS) into pyrite (FeS_2):

$$Fe^{2+} + S^{2-} \rightarrow FeS \tag{4.9}$$

(El-Hajj, *et al*., 2013)

$$FeS_2 + 14Fe^{3+} + 8H_2O \rightarrow 15\ Fe^{2+} + 2\ SO_4^{2-} + 16H^+ \tag{4.10}$$

(Bottrell and Raiswell, 2000)

Consistent with the visual inspections of the added corrosion coupons, black FeS-films were observed to have developed, possibly suggesting the transformation of Fe^{2+} and S^{2-} into FeS (Equations 4.9–4.10). From microbially enhanced oil recovery (MEOR) in reservoir rock sands experiments, a consistent observation to the previous notion of *Halanaerobium* sp. fermentative metabolism pathways, whereby 1% pyrite and calcite enhanced the enriched *Halanaerobium* sp. fermentative metabolism of sucrose yielding sixfold higher acetate production rates compared to quartz sand (Kögler, *et al*., 2021).

4.4.2 Salinity Effect on Sulphate Reduction, Sulfidogenesis, and Methanogenesis from (ISW:PW) – Microbial Dynamics Perspective

Salinity increases in ISW:PW mixes from the NS water production system (127 g/L TDS) and the AG water production system (204 g/L TDS) across the thermal gradient (15°C–60°C) had a major impact on increasing sulphide depletion rate (mM/hrs.) (Figure 4.4), increasing maximum sulphide depletion (Figure 4.6), and under than the stoichiometric amounts of headspace CH_4 production from VFA metabolism (Figure 4.7). The positive control for sulfidogenesis (100% ISW) (42 g/L TDS), however, exhibited a rapid sulphide production profile (18.05 mM ± 0.11) (Figure 4.1). This was consistent with the follow-up experiment that demonstrated that the salinity threshold for sulfidogenesis induced by SRP under the synthetically prepared water production systems mesophilic incubations (30°C) was 107 g/L TDS and was 64 g/L TDS for moderate thermophilic incubations (60°C) (Sindi, *et al*., 2021). Additionally, earlier literature also reported that the mesophilic (30°C) acetoclastic methanogens did not grow when NaCl concentrations exceeded 50 g/L (Blake, *et al*., 2020). The thermodynamics limit for microbial life in the deep biosphere (including sulphate-reducers) under high salinity conditions was proposed by Oren (1999, 2001, 2011). In these literature studies, it was proposed that microbial life at high salt concentrations was energetically expensive. Therefore, for microbial life to thrive, the following factors must be considered: A) The energy amounts generated from the dissimilatory metabolism and B) The mode of osmotic adaptation. These are consistent with some of the findings reported in this experiment; whereby: for instance, under the (100% ISW-30°C) incubations; sulphide production occurred most likely coupled with VFAs metabolism energy channelled into sulphate reduction into sulphide (Figure 4.1) (Equations 4.1–4.3). Additionally, the literature reported mode of osmotic adaptations for the enriched *Halanaerobium* sp., and with which production of osmoprotectant compounds such as (Betanin-glycine) would allow them to pump out the intracellular cations and anions (typically K+ and Cl-), to survive the osmotic pressure (Oren, 2011).

Halanaerobium sp. were enriched in both the NS water production system (127 g/L TDS) and the AG water production system (Max: 31.02 ± 2.34%; Max: 25.3± 1.62%, respectively) (Figure 4.15a,b), with higher diversity in the AG water production system (204 g/L TDS) (Figure 4.15). A literature survey of the higher salinity adaptive capabilities for the enriched *Halanaerobium* sp. is displayed in Table 4.3.

Higher salinity adaptive capability for the selected and literature-reported novel isolated *Halanaerobium* sp. was displayed (Table 4.3). This higher salinity adaptive

TABLE 4.3
Literature Survey on Selected Novel Isolated *Halanaerobium* sp.

Species/Genus	Isolation Habitat	Salinity Range for Growth	Optimum Growth Temperature	VFAs Produced from Carbohydrates Fermentation	References
Halanaerobium sehlinense sp.	surface Sabkha Sediments (Tunisia)	*20% 5–30% 50–300 g/L (NaCl)	**43°C 20–50°C	Lactate, acetate, formate	Abdeljabbar, *et al*. (2013)
Halanaerobium congolense sp.	Oil well-head sample (Republic of Congo)	10% (100g/L) (NaCl)	**42°C	Acetate	Ravot, *et al*. (1997)
Halanaerobium Kushneri sp.	Petroleum reservoir fluid, Oklahoma (U.S.A)	*15–20% (150–200 g/L) (NaCl)	37°C	Acetate and formate	Bhupathiraju, *et al*. (1999)

* Optimal Growth Salinity
** Optimal Growth Temperature

capabilities for the novel isolated *Halanaerobium* sp. reported in earlier literatures were in range with the reported *Halanaerobium* sp. enrichments from this experiment's (ISW:PW) synthetic mixes mimicking the NS water production system (127 g/L TDS–12.7% TDS), and the AG water production system (204 g/L TDS–20.4% TDS) (Figure 4.15a,b). Additionally, the mesophilic incubation (30°C) parameter was also in range with the literature-reported growth temperature range (20–50°C) for the novel isolated *Halanaerobium* sp. (Table 4.3). At the higher thermophilic incubating temperatures (45°C–60°C) of the (NS-PW 127 g/L TDS) and the (AG-PW 204 g/L TDS) ISW:PW mixes, *Halanaerobium* sp. *16S rRNA* sequences were not detected, with the rest of the detected sequences making up only between (1%–4% RA), and therefore not showing much microbial activity or eliciting a major population shift (Figure 4.16a–c); (Figure 4.17a–c).

4.4.3 Impact of Salinity on *Halanaerobium* sp. Enrichments

Halanaerobium sp. were isolated from field production waters in MEOR evaluation experiments (Kögler, *et al*., 2021). The isolated *Halanaerobium* sp. grew on nutrient media supplemented with sucrose, dried yeast extract, and molybdate (also SRB growth inhibitor) as carbon source and did not show evidence of sulfidogenesis nor extensive MIC (Kögler, *et al*., 2021). Indeed, *Halanaerobium* sp. have previously been also detected in a range of medium to high salinity-produced waters (Booker, *et al*., 2017; Vilcaez, *et al*., 2018).

In another study, Vilcaez *et al*. (2018) conducted an anoxic microcosm experiment to study methanogenic crude oil biodegrading microorganisms. In their study, the anoxic microcosms were prepared from the Stillwater and Crushing oilfields of Oklahoma, USA, supplemented with a nutrient solution containing a mixture of

basal salts, without sulphate. Additionally, a protein-rich matter (i.e., amino acid source) was used as the carbon source for microbial metabolism. Vilcaez *et al*. (2018) reported the detection of *Halanaerobium* sp., in high salinity still water formation (116.7 g/L) and higher salinity formation water (285.76 g/L). Microbial community analysis for the low salinity still water formation revealed 46% relative abundance of *Marinobacter*, and 21.5% relative abundance of *Halanaerobium* and *Acetohalobium* in water sample prior to incubation. However, at the end of the incubation period, *Marinobacter, Halanaerobium*, and *Acetohalobium* could no longer be detected. Instead, *Deferribacter*, (49.9%), *Geotoga*, *Kosmotoga*, and *Petrotoga* (14.9%) were enriched. These constituted only about 9.3% relative abundance of the microbial communities at the start of incubations. On the other hand, the microbial communities in the high salinity formation water at the start comprised 33.4% of *Actinobacteria* (genus *Propionibacterium*), with 26.9% comprising *Acinetobacter, Marinobacter, and Halomonas*; 14.2% of the genera *Staphylococcus, Streptococcus, Bacillus*, and *Halanaerobium*; and 8.9% *Achromobacter*, and *Pelomonas*. At the end of incubations, however, only, three lineages were detected, which constituted 98.7% of the microbial community. Those lineages belonged to *Deferribacter* (23.4%), *Kosmotoga* (13.5%), and *Candidatus Schekmanbacteria* (61.7%). A point of similarity between the study conducted by Vilcaez, *et al*., (2018) and our current study was the selective enrichment of *Halanaerobium* sp. under high salinity production water conditions. No sulphate was supplemented to growth media as an electron acceptor (Vilcaez, *et al*., 2018), and like our experiment, the supplemented sulphate was not reduced under both (20:80%) ISW:PW (NS) and (20:80%) ISW:PW (AG) incubations. The metabolism for *Halanaerobium* sp., which occurred in the study of (Vilcaez, *et al*., 2018), was possibly due to the consumption of the protein-rich matter and/or the organics in crude oil (without addition of sulphate as a terminal electron acceptor). In contrast, sugar fermentation metabolism pathways for *Halanaerobium* sp. selective enrichment in our PWRI most likely occurred, with VFAs production, and with no significant sulphate reduction (i.e., terminal electron acceptor). However, the contribution of River Tyne organic matter as a carbon source for the enrichment of *Halanaerobium* sp. would require further investigations.

Halanaerobium sp. has been identified in a wide range of oil fields from the Gulf of Mexico (Scheffer, *et al*., 2021), the Permian Basin-U.S.A (Tinker, *et al*., 2022) to an offshore oil field in the Republic of the Congo in Africa "*Halanaerobium congolense*" (Ravot, *et al*., 1997) (Table 4.3). Tinker, *et al*. (2022) have recently demonstrated that *Halanaerobium* sp. was an integral component of the microbiome of the Permian Basin, the highest oil- and gas-producing reservoir in the United States. The *16s rRNA* gene sequencing and metagenomic analysis revealed that microbiome of the Permian basin was dominated by sulphate and thiosulfate-reducing taxa including: *Halanaerobium* sp.*, Orenia* sp.*, Marinobacter* sp., and *Desulfohalobium* sp., and that there was a high prevalence of sulphate and thiosulfate-reducing genes in metagenome-assembled genomes (MAGs) assembled from the metagenome sequences.

Permian Basin produced water samples had Total Dissolved Solids (TDS) concentrations in the range of (110 g/L–107 g/L), and, therefore, slightly under this experiment's (20:80%) (ISW:PW) (NS) (127 g/L TDS) salinity. From these ISW:PW

incubations, the relative abundance of *Halanaerobium* sp. enrichments in the (NS) water production system was: 22.58 ± 1.23% (Max. at 15°C); and 31.02 ± 2.34% (Max at 30°C), and similar to the relative abundance of *Halanaerobium* sp. reported in the Permian basin produced water samples of (RA 33.58%) (Tinker, *et al*., 2022).

4.4.4 Impact of Salinity and Temperature on *Halanaerobium* sp. Enrichments

Booker *et al*. (2017) monitored the enrichment of *Halanaerobium* sp. from the input fluids prior to down-hole injection for hydraulic fracturing operations at the Utica shale well in Ohio, United States. The monitoring revealed strong enrichment of *Halanaerobium* sp. (99% relative abundance in *16S rRNA* gene libraries), at 100 days post-injection. A *Halanaerobium* sp. isolated from the Utica shale well was grown on a defined saltwater liquid medium containing a range of basal salts, making up ~113 g/L salinity. The medium was amended with 10 mM thiosulfate ($Na_2S_2O_3.5H_2O$), as the terminal electron acceptor for *Halanaerobium* sp., growth, and with D-glucose as the carbon source for *Halanaerobium* sp. growth. Further evidence from the literature suggested that *Halanaerobium* sp. is a dominant and colonising microbial taxon across a range of wells and shale plays (Choudhary, *et al*., 2015; Daly, *et al*., 2016; Liang, *et al*., 2016; Lipus, *et al*., 2017).

Halanaerobium sp. was recently found to be an integral part of the produced water microbiome of the Gulf of Mexico (Scheffer, *et al*., 2021). Ravot *et al*. (1997) were the first to report the isolation of a *Halanaerobium* sp., from an offshore oil field in the Republic of the Congo in Africa, hence the name "*Halanaerobium congolense*." *Halanaerobium congolense* grew optimally at 42°C and a pH of 7 (Table 4.3). No growth was observed at temperatures below 20°C, and above 45°C, like the experiment where the selectively enriched *Halanaerobium* sp. grew at 15°C and 30°C but not at 45°C or 60°C (Figure 4.15a,b). The pH range for the growth reported by Ravot *et al*. (1997) was between 6.3 and 8.5, and pH in our experiment was in that range at the pH value of 7.5, and remained constant, throughout the experiment. This strain was able to ferment a range of carbohydrates, including fructose, galactose, D-glucose, maltose, D-mannose, D-ribose, sucrose, trehalose, and bio-tryptase. However, strain SERB 4224, isolated by Ravot *et al*. (1997), did not utilise D-arabinose, lactose, rhamnose, D-xylose, dulcitol, acetate, butyrate, propionate, and lactate. Under a pure culture enrichment experimental setting, the ability of a *Halanaerobium congolense* sp. to produce biofilms and sporulate was reported (Jones, *et al*., 2021).

4.4.5 Estuarine River Tyne Sediments Microbial Processes

Sulphate reduction and methanogenesis were the electron-accepting processes evaluated under this experiment (Figures 4.3 and 4.7, respectively). This was achieved via aqueous sulphate and the microcosms headspace methane production. Results revealed no sulphate reduction and therefore no sulfidogenesis under both the NS and the AG water production systems (127 g/L) and (204 g/L), respectively, and across the incubation temperature gradients (15°C–60°C). Minimal headspace methane

(CH_4) production amounts were observed (nmoles opposed to mmoles) ruling out the contribution of methanogenesis as a potential electron-accepting process.

Methanogenesis is an important microbial process occurring in natural environments, such as River Tyne estuarine sediments (Blake, *et al*., 2020). Under a range of similar salinity and temperature gradients, and using River Tyne Estuarine sediments for microbial inoculum, the enrichments of methanogens were reported by Blake, *et al*. (2020). The enriched methanogens could grow at both low (5°C–30°C) and high (40°C–70°C) incubating temperatures, and in both (CO_2/H_2) headspace amended and unamended microcosms. Compared to these ISW:PW experiments, under the NS (PW) and the AG (PW) incubations (127 g/L TDS) and (204 g/L TDS), respectively, minimal sulfidogenesis was occurring under the NS (PW) (2 mM – 40 days), and no sulfidogenesis occurring at the AG (PW) (0 mM – 40 days), no methane was detected in the headspace (Figure 4.7), and no methanogenic enrichments were detected under the tested (NS) and the (AG) ISW:PW mixes incubations (Figures 4.12 and 4.13, respectively).

Recently, the definition of "Palaeopickling" was proposed by Head, *et al. (*2014). This definition is pertinent to reservoir sterilisation because of extreme reservoir temperature and salinity gradients. At such extreme salinity and temperature gradients, the maximum temperature threshold for microbial growth and flourishment under extreme reservoir conditions can be lower at elevated salinities (Head *et al*., 2014). To survive the extreme reservoir salinity gradients, reservoir microorganisms would deploy one of two mechanisms (Head, *et al*., 2014). Firstly, the intracellular accumulation of ions (typically K^+ and Cl^-) countering the extracellular high salinity reservoir conditions. Secondly, the intercellular synthesis of compatible solutes was proposed to counter the salinity effect (Oren, 1999). In both cases, a considerable expenditure of energy will be required, which will be deducted from the energy channelled for primary metabolism (Oren, 2011).

Estuarine sediments are also known to have substantial amounts of elemental sulphur (Viggi, *et al*., 2017), and River Tyne sediments are no exception. In a more general sense, aquatic marine sediments were reported to have both thiosulfate and elemental sulphur thiosulfate ($S_2O_3^{2-}$) (0–100 µM) range (Jørgensen, 1990); Sulphur (S^0) (200–1600 µM) (Mitchell, *et al*., 1988). Consequently, a continuous shuttle of oxidised or reduced sulphur-species forms, including thiosulfate, may occur under such sedimentary systems (Viggi, *et al*., 2017). Therefore, the S-species reported concentrations in aquatic marine sediments (~2 mM) matched the reported sulphide production (mM) concentrations for (20:80%) ISW:PW (NS) (~127 g/L) reported in this experiment (~2 mM) (Figure 4.2). Additionally, the literature reported S-species in aquatic marine sediments could have provided the required electron acceptor for the low-temperature-driven *Halanaerobium* sp. enrichments in this experiment. Two potential sources of thiosulfate presence in microcosms as a terminal electron acceptor in this study are from: firstly, medium-sediment particulates interactions, which may represent the real-field thiosulfate releasing mechanism from hydraulic shale, as a result of the interactions of hydraulic fracturing fluids with reservoir rocks (Danika, *et al*., 2021), secondly, the detection of *Sulfurovum* sp. sequences under all low- and high-temperature microcosms (Figure 4.16b); Figure 4.17b is implicated in sulphur oxidation, as reported by Mori *et al*. (2018). This was manifested by the reported

Novel *Sulfurovum* sp. to oxidise sulphide via using thiosulfate and elemental sulphur as electron donors, and with the ability to use oxygen and nitrate as electron acceptors (Mori, *et al*. 2018). An additional thiosulfate source in hydraulic fracturing operations would be the hydraulic fracturing chemical additives added to the mud mixtures in prior to downhole field injections. Sediment-rock interactions represent a long-term reservoir of thiosulfate supporting the microbial metabolism when the thiosulfate from hydraulic fracturing chemical additives is depleted. However, the processes may represent a cryptic cycle and rapid turnover events of sulphur compounds, which consequently would limit the understanding of the true extent of thiosulfate transformation over the monitoring period. The Aarhus Bay marine sediments were a good source of microbial inoculum, harbouring a great microbial diversity and, therefore, used in SRP reaction rates study (Holmkvist, *et al*., 2011). In that study, a cryptic S-species cycle in both the sulphide and methane zones of marine sediments was proposed (Holmkvist, *et al*., 2011). This cryptic S-species cycle was manifested in the sedimentary deposition and reaction of Fe (III) minerals with sulphide. Together and in combination with sulphur disproportionation, a quantifiable conversion of sulphide to pyrite was observed (Holmkvist, *et al*., 2011). Sulphate and thiosulfate are known intermediates of the S-species cryptic cycles and, therefore, marine sediments would provide a plausible source of alternative electron acceptors in marine sediment systems, which might be occurring in parallel with the fermentation of complex organic matter in marine sediments and therefore supporting the low-temperature (15°C–30°C) microcosms *Halanaerobium* sp. enrichments under in this study (Figure 4.15a,b, respectively).

4.4.6 Implications of *Halanaerobium* sp. in Oil and Gas Industry Processes and Practices

Numerous microbiology studies in hydraulic fracturing fluids have found that microorganisms can grow in the newly fractured hydraulic shales and persist over an extended period, leading to a series of deleterious consequences such as souring (production of H_2S), MIC, production of biogenic gasses, and pore plugging (Murali, *et al*., 2013a, 2013b). In some cases, *Halanaerobium* sp. were found to be enriched to levels where they contributed 99% of the *16S rRNA* gene sequences in *16S rRNA* gene libraries from flow-back waters and detected as a key member in production fluids (Daly, *et al*., 2016; Mouser, *et al*., 2016; Murali, et al., 2013b). It has also been shown that supplementing hydraulic fracturing fluid samples with thiosulfate resulted in enrichment of *Halanaerobium* sp. (Booker, *et al*., 2017).

Scale formation is another common problem in the oil and gas industry. Initially, it can coat perforations, casing, and tubing. If allowed to further develop, it could lead to limiting the production, and eventually the abandonment of the well. Referring to the enrichment of *Halanaerobium* sp. under high salinity produced water fluids, it has been proposed that this could be happening in the fractured shales in the Appalachian basin, due to the insufficient energy yields (carbon source) to synthesise osmoprotectants and reduce sulphate simultaneously for SRB (high salinity growth requirements), in comparison with the fermentative *Halanaerobium* sp. growth and adaptability under high salinity conditions (Oren, 2011).

To curtail the growth and enrichment of microbes with MIC-potential, biocide chemicals are usually administered in numerous oil and gas industry processes and practices. Current biocidal application practices during the PWRI process, for instance, often involve alternating biocidal treatments using different chemical formulations, and these often need to be reviewed every 2–3 years due to the possible biocidal inefficacies because of microbial resistance. Incorporating field-specific temperature and salinity gradients in biocide efficacy testing before field applications will aid in the better understanding of the possible emergence of biocidal microbial resistance creating multiple lines of benefits for the industry, such as cost avoidance (CAPEX and OPEX), reduced crude processing costs, reduced downtime, and safety benefits.

4.4.7 *Halanaerobium* sp. S-species Respiratory Pathways

Aquatic marine sediments have been reported to have hugely varying concentrations of thiosulfate ($S_2O_3^{-2}$), and elemental sulphur (S^0). Some literatures reported the detection of the high concentrations of: (0–100 μM) range for (Thiosulfate (($S_2O_3^{2-}$) (Jørgensen, 1990); Sulphur (S^0) (200–1600 μM) (Mitchell, *et al*., 1988), while other literature reported much lower quantities of: (≥0.5 μM) for both thiosulfate and elemental sulphur) (Zopfi, *et al*., 2004). Potentially, the reported systematic sulphide depletion profiles from this ISW:PW incubations suggested that the depleted sulphide was oxidised; possibly via the manganese oxides (Mn (IV)) and iron oxides Fe (II) oxides), producing preliminary elemental sulphur (S^0) (Pyzik and Sommer, 1981; Yao and Millero, 1993, 1996). Sulphur (S^0) is produced as an intermediate or final product during bacterial oxidation of sulphide and thiosulfate (Schippers and Jørgensen, 2001), and microorganisms produce (S^0) as an intermediate or final product during oxic and anoxic iron sulphide (Fes) oxidation (Schippers and Jørgensen, 2001). The ability of *Halanaerobium* sp. to utilise S-species as a terminal electron acceptor stem from the presence of protein-coding *Rhodanese* enzymes genes in their genome, and their capabilities to upregulate the expression of these *Rhodanese* enzymes coding-genes, including one of the three subunits of the anaerobic sulphite reductase enzyme (*AsrA*). Below equations illustrate the reaction catalysed by *Rhodanese* enzymes (Equation 4.12) and the anaerobic sulphite reductase (Equation 4.13):

$$S_2O_3^{2-} \rightarrow SO_3^{2-} + S^0 \tag{4.12}$$

$$SO_3^{2-} + NADH \rightarrow H_2S + NAD^+ + 3H_2O \tag{4.13}$$

Halanaerobium sp. capabilities also included their ability to outcompete SRB on energy sources (Booker, *et al*., 2017). This was due to the need but insufficiency of SRB to produce osmoprotectants from the energetic yields of sulphate reduction to maintain their growth. During *Halanaerobium* sp. growth phase, electron donors are oxidised, and the energy coupled to the desirable for growth electron acceptor (e.g., S^0, $S_2O_3^{2-}$, SO_3^{2-}) Furthermore, Booker, *et al*. (2017) suggested that during the stationary growth phase of the *Halanaerobium* sp., sulphite-reduction would not be coupled to growth but rather as a disposal mechanism for the fermentation reducing

equivalents, such as ethanol, acetate, and formate. This was done following a proteomics analysis approach to determine the proteins produced from biomass during the stationary growth phase of *Halanaerobium* sp. The reported *Rhodanese* enzymatic machinery present in *Halanaerobium* sp. genome would explain the enrichment of this species under (20:80%) ISW:PW (NS) (127 g/L TDS) and (20:80%) ISW:PW (AG) (204 g/L TDS) systems, whereby one of three possibilities occurred: A) The literature reported thiosulfate, sulphur and potentially present in River Tyne Estuarine marine sediments were utilised as electron acceptors for *Halanaerobium* sp. Respiration, and B) The observed depleted and potentially turned-over sulphide could have worked as electron acceptor under this specific ISW:PW experimental setup (Figure 4.1), and C) The complex organic matter present in River Tyne Estuarine marine sediments at varying concentrations, including carbohydrates, were fermented into VFAs by the enriched *Halanaerobium* sp. (Figure 4.15a,b).

4.4.8 *Halanaerobium* sp.-Induced Microbial Contamination and Control Mechanisms

Halanaerobium sp. can grow and adapt to the rapid shifts in physicochemical conditions of the hydraulic fractured (HF) fluids due to their network of metabolic functions, cantered around the cycling of osmoprotectants and methylamine compounds (Borton, *et al*., 2018; Liang, *et al*., 2016). The direct growth advantage of *Halanaerobium* sp. includes their ability to catalyse thiosulfate-dependent sulfidogenesis (Booker, *et al*., 2017), and growth on HF fluid additives (Borton, *et al*., 2018; Daly, *et al*., 2016; Liang, *et al*., 2016), to potentially form biofilms. Such biofilms could directly lead to bio clogging, and biofouling but could, on the other hand, have a positive impact on sealing the cap-rocks in geologic CO_2-sequestration reservoirs (Mitchell, *et al*., 2008). Liang *et al*. (2016) demonstrated the ability of *Halanaerobium* sp. strain (DL-01) to consume (degrade) guar gum and produce acetate. A series of biocides efficacies was determined against the isolated and tested *Halanaerobium* sp. (DL-01) and showed that Quaternary Ammonium Compounds (QAC) biocide was the best biocide in controlling the growth of *Halanaerobium* sp. in the presence of thiosulfate, followed by glutaraldehyde, and finally Tetra Hydrokis Phosphonium Sulphate (THPS). These reported observations, and with the salinity and temperature gradients reported from this experiment demonstrate the ability of *Halanaerobium* sp. to utilise the more complex carbon sources, such as guar gum Liang *et al*. (2016), and potentially the more complex organic matter present in River Tyne sediment, either solely or as part of the mixed microbial community's synergist relationships. The latter, however, would require further investigations to confirm.

4.4.9 The Relevance of Other Microbial sp. Enrichments under PWRI Physicochemical Parameters

From the current study, the consistent presence of *Woeseia* sp., under both low-temperature incubations (15°C and 30°C) (Figure 4.16a) and high-temperature incubations (45°C and 60°C) Figure 4.17a suggests that this species may be one of the integral constituents of Tyne sediments microbiome in specific and the global

estuarine sediments microbiome in general. Indeed, the literature reported numerous incidences where *Woeseia* sp. sequences were detected in estuarine sediments using *16S rRNA* Next-Generation Sequencing (NGS) in Shuangtaizi River, China (Zhang, *et al*., 2021), coastal sediments (Malva-rosa beach) (Valencia, Spain) (Vidal-Verdú *et al*., 2022), and seafloor sediment communities (Hoffmann, *et al*., 2020), with the utilisation of protein-based microbial cell-components, and other microbial organic remnants as a carbon source for their metabolism. Additionally, the enrichment of *Sulfurovum* sp. under all low- and high-temperature treatments could have potentially led to sulphur oxidation, coupled with the reduction of a suitable electron acceptor (e.g., Oxygen and Nitrate) as reported by (Mori, *et al*., 2018). Therefore, contributing to a potential S-species cryptic cycle.

4.4.10 The Observed Pitting Nucleations

From these ISW:PW incubations, low general corrosion rates of <0.02 (mm/yr.) were reported across the tested thermal gradient of (15°C–60°C) (Figure 4.8a,b). However, the occurrence of advance-staged pitting nucleations was reported for both 20:80% (ISW:PW) (NS) (127 g/L TDS) (30°C) incubations and 20:80% (ISW:PW) (NS) (127 g/L TDS) (60°C) (Figures 4.9 and 4.10). Lower number of pitting nucleations with smaller diameter (per cm^2) were reported under the NS water production system (30°C) incubations (0.17–0.22 pits of 20 μm,), compared against the higher numbers of pitting nucleations with larger diameter (per cm^2) for under the NS water production system (60°C) incubations (and 1400 pits of 50 μm–150 μm) (Figure 4.9). Additionally, different pitting nucleation morphologies were detected for (30°C) (NS) incubations, possibly suggesting the co-occurrence of multiple pitting corrosion mechanisms (Figures 4.9 and 4.10, respectively) for the reported wide-shallow pitting nucleations and the sub-surface nucleations. Due to the nature of the conducted ISW:PW experiments, however, and whereby a mixture of physical-chemical parameters is tested at once, it would prove difficult and therefore require further investigations to pinpoint the root cause of the reported advance-staged pitting nucleations. In corrosion experiments conducted on stainless steel (more-corrosion-resistant alloy than carbon steel), three key factors were reported to be detrimental for the development of pitting corrosion (chloride, temperature, and pH) (Dastgerdi, *et al*., 2019). When increasing the concentrations of chloride ions, increasing temperature, and pH; a general decrease in localised corrosion resistance of stainless steel usually occurs (Dastgerdi, *et al*., 2019; Ramana, *et al*., 2009). Therefore, in ISW:PW systems whereby a mixture of biotic (i.e., microbes implicated in MIC) and abiotic (i.e., Chloride, temperature, and pH) factors interact, the cumulative and individual contributions of such factors in the potential general corrosion, localised corrosion (e.g., pitting), and the associated corrosion depth (e.g., corrosion pits depth) would require further investigations.

4.5 CONCLUSIONS

A fundamental anoxic microcosm experiment was conducted to understand the effects of higher salinity synthetic ISW and synthetic PW mixing on sulphate reduction, sulphide production, methanogenesis, general corrosion potential, localised

corrosion potential, and the associated microbial community dynamics. The fundamentally tested synthetic ISW and synthetic PW mixes represented oil and gas industry mixing scenarios for ISW and PW such as: A) On-shore oil production facility water flooding lines, B) On-shore oil production facility ISW:PW mixing tanks, C) Off-shore platforms ISW:PW mixing tanks, and D) Oil reservoir ISW:PW mixing zone. A summary of the main conclusions from these ISW:PW incubations, followed by the broader implications are shown below:

- Salinity had a major impact on microbial sulphate reduction, whereby under 20:80% ISW:PW (NS) (127 g/L TDS) thermal gradient (15°C–60°C) incubations, and 20:80% ISW:PW (AG) (204 g/L TDS) thermal gradient (15°C–60°C) incubations, sulphate reduction did not occur but rather remained stable throughout incubation timeframes (NS, average 4.6 ± 0.38 mM sulphate; AG, 9.8 ± 0.60 mM sulphate, Figure 4.3).
- A systematic sulphide depletion profile for (with coupon) 20:80% ISW:PW thermal gradient (15°C–60°C) incubations from the NS and from the AG was reported (NS average sulphide depletion: 2.63 ± 0.23 (Figure 4.6a); AG average sulphide depletion: 2.15 ± 0.32) (Figure 4.6b), possibly suggesting the transformation of the depleted sulphide into iron sulphide (FeS) biotically or abiotically.

Under 100% ISW (without coupon) (NS-30°C) (42 g/L TDS) incubations, however, a rapid sulphide production profile was reported (18.05 mM ± 0.11 (Figure 4.1).

- The SRP microbial communities under 100% ISW (without coupon) (NS-30°C) (42 g/L TDS) incubations, most likely coupled their sulphate-reduction respiration into sulphide with the added VFAs metabolism (Figure 4.1).
- The observed shifts in microbial communities from the potential SRP communities under (100% ISW (without coupon) (NS-30°C) (42 g/L TDS) incubations into members of *Halanaerobium* sp. suggest changes in metabolism pathways from (VFAs-sulphate) anaerobic SRP respiration, into thiosulfate reduction or carbohydrates fermentation pathways for *Halanaerobium* sp. (Figure 4.15a,b).
- The possibility for the occurrence of another electron-accepting process (e.g., hydrogenotrophic and acetoclastic methanogenesis) was investigated. Methane headspace (CH_4) mass results ruled out the presence of (mmoles) amounts to drive the (VFAs-methane) stoichiometric conversions (Figure 4.7).
- Gravimetric analysis of corrosion coupons revealed low corrosion rates of <0.02 (mm/yr.) for both the 20:80% ISW:PW (NS) (127 g/L TDS) thermal gradient (15°C–60°C) incubations and the 20:80% ISW:PW (AG) (204 g/L TDS) thermal gradient (15°C–60°C) incubations (Figure 4.8a,b).
- Surface morphology analysis revealed the development of advanced-stage pitting nucleations on corrosion coupon surface for 20:80% ISW:PW (NS) (30°C) (0.17–0.22 pits of 20 μm) and 20:80% ISW:PW (NS) (60°C)

(1400 pits of 50 μm–150 μm), for pits number and diameter per cm^2, respectively) (Figure 4.9).
- Elemental composition of corrosion coupons for 20:80% ISW:PW (NS) (30°C), and 20:80% ISW:PW (NS) (60°C) incubations revealed the potential presence of both phosphate and carbonate deposits, based on the ionic composition (%) of carbon, oxygen, and phosphorus elements (Table 4.2).

The oil and gas industry faces great difficulties in terms of pinpointing field-specific microbiological contamination or microbiological issues. This is caused by reservoir microorganisms' adaptive capabilities to live under harsh reservoir environments (e.g., temperature, salinity, and pressure). Tending to live in microbial communities and clusters (e.g., biofilms), synergistic microbial reaction effects can be evident. To overcome the dilemma of field-specific microbiological contamination, a few pointers were proposed in this chapter. Firstly, multiple layers of geochemical, microbiological, and metallurgical test results must be considered before pinpointing the root cause, and field-specific microbiological issues causative agent. Secondly, the oil and gas industry processes and practices such as PWRI and HF must be considered in these systematic lab experiments, together with the multiple layers of test result evidence. For example, actively growing reservoir microorganisms may be re-injected in an open-loop system during PWRI and HF operations, and whereby continuous provision of suitable nutrients, electron donors, and electron acceptors are achieved. Thirdly, to unravel the mystery of field-specific microbiological contamination/issues, and prolong biocidal efficacies in the field programs, the field-specific salinity and temperature gradients must be implemented within the lab-based biocidal efficacy studies. Therefore, enhancing the effects of the field-applied biocidal chemistries in curtailing the growth and activity of the detrimental microorganisms for the subject field application. Finally, with the advent of NGS and bioinformatics capabilities, field-specific microbiological contamination/issues can be incorporated with the above pointers, aiding towards microbial characterisations and envisioned microbial functions discovery (proteomics). Therefore, a holistic approach aimed at incorporating the pointers would prove vital as proactive approach and may be implemented within microbiological best field practices documents. Therefore, curtailing the growth and activity of microorganisms implicated in oil and gas industry operations.

ACKNOWLEDGEMENTS

We would like to acknowledge the book editors Biwen Annie An Stepec, Torben Lund Skovhus, and Kenneth Wunch for useful discussions on this research during the ISMOS-8 conference and editing of the chapter. The appreciation is extended to colleagues within the Electron Microscopy Research Services, Newcastle University, for conducting the SEM/EDS analyses; Henriette Christensen for conducting ion chromatography for anions; Mark Hedley for microbial community analysis discussions; and Saudi Aramco's Research & Analytical Services Department Management for encouragement and financial support.

REFERENCES

Abdeljabbar, H., Cayol, J.L., Ben Hania, W., Boudabous, A., Sadfi, N. and Fardeau, M.L., (2013). *Halanaerobium sehlinense sp*. nov., an extremely halophilic, fermentative, strictly anaerobic bacterium from sediments of the hypersaline lake Sehline Sebkha. *International Journal of Systematic and Evolutionary Microbiology*, ***63***(Pt_6), pp. 2069–2074.

Angelidaki, I., Karakashev, D., Batstone, D.J., Plugge, C.M. and Stams, A.J., (2011). Biomethanation and its potential. In *Methods in enzymology* (Vol. 494, pp. 327–351). Academic Press.

Bader, M.S.H., (2007). Sulfate removal technologies for oil fields seawater injection operations. *Journal of Petroleum Science and Engineering*, ***55***(1–2), pp. 93–110.

Bhupathiraju, V., McInerney, M.J., Woese, C.R. and Tanner, R.S. (1999). *Haloanaerobium kushneri sp. nov*., an obligately halophilic, anaerobic bacterium from an oil brine. *International Journal of Systematic Bacteriology*, ***49***, pp. 953–960.

Bjørlykke, K., Aagaard, P., Egeberg, P.K. and Simmons, S.P., (1995). Geochemical constraints from formation water analyses from the North Sea and the Gulf Coast Basins on quartz, feldspar and illite precipitation in reservoir rocks. *Geological Society*, London, Special Publications, ***86***(1), pp. 33–50.

Blake, L.I., Sherry, A., Mejeha, O.K., Leary, P., Coombs, H., Stone, W., Head, I.M. and Gray, N.D., (2020). An unexpectedly broad thermal and salinity-tolerant estuarine methanogen community. *Microorganisms*, ***8***(10), p.1467.

Booker, A.E., Borton, M.A., Daly, R.A., Welch, S.A., Nicora, C.D., Hoyt, D.W., Wilson, T., Purvine, S.O., Wolfe, R.A., Sharma, S. and Mouser, P.J., (2017). Sulfide generation by dominant *Halanaerobium* microorganisms in hydraulically fractured shales. *M Sphere*, ***2***(4), pp. e00257–17.

Booker, A.E., Hoyt, D.W., Meulia, T., Eder, E., Nicora, C.D., Purvine, S.O., Daly, R.A., Moore, J.D., Wunch, K., Pfiffner, S.M. and Lipton, M.S., (2019). Deep-subsurface pressure stimulates metabolic plasticity in shale-colonizing *Halanaerobium spp*. *Applied and Environmental Microbiology*, ***85***(12), pp. e00018–19.

Borton, M.A., Hoyt, D.W., Roux, S., Daly, R.A., Welch, S.A., Nicora, C.D., Purvine, S.O., Eder, E.K., Hanson, A.J., Sheets, J.M., Morgan, D.M., Sharma, S., Carr, T.R., Cole, D.R., Mouser, P.J., Lipton, M.S., Wilkins, M.J., Wrighton, K.C., (2018). Coupled laboratory and field investigations resolve microbial interactions that underpin persistence in hydraulically fractured shales. *Proceedings of the National Academy of Sciences of the United States of America*, ***115***, pp.E6585–E6594. doi:10.1073/pnas.1800155115

Bottrell, S.H. and Raiswell, R., (2000). Sulphur isotopes and microbial sulphur cycling in sediments. *Microbial Sediments*, pp. 96–104.

Chen, C., Shen, Y., An, D. and Voordouw, G., (2017). Use of acetate, propionate, and butyrate for reduction of nitrate and sulfate and methanogenesis in microcosms and bioreactors simulating an oil reservoir. *Applied and Environmental Microbiology*, ***83***(7), pp. e02983–e02916.

Choudhary, L., Macdonald, D.D. and Alfantazi, A., (2015). Role of thiosulfate in the corrosion of steels: a review. *Corrosion*, ***71***(9), pp. 1147–1168.

Cord-Ruwisch, R., (1985). A quick method for the determination of dissolved and precipitated sulfides in cultures of sulfate-reducing bacteria. *Journal of Microbiological Methods*, ***4***(1), pp. 33–36.

Daly, R.A., Borton, M.A., Wilkins, M.J., Hoyt, D.W., Kountz, D.J., Wolfe, R.A., Welch, S.A., Marcus, D.N., Trexler, R.V., MacRae, J.D. and Krzycki, J.A., (2016). Microbial metabolisms in a 2.5-km-deep ecosystem created by hydraulic fracturing in shales. *Nature Microbiology*, ***1***(10), pp. 1–9.

Danika, N., Subasthika, T. and Gieg, L., (2021). Microbial corrosion under thio-sulfate reducing conditions by microbial communities in hydraulically fractured shale flowback waters. In *8th International Symposium on Applied Microbiology and Molecular Biology in Oil Systems*. p.39. Abstract Book available at: https://ismos-8.org/wp-content/uploads/2021/06/07062021_ISMOS-8_ABSTRACT-BOOKFINALFINAL.pdf

Dastgerdi, A.A., Brenna, A., Ormellese, M., Pedeferri, M. and Bolzoni, F., (2019). Experimental design to study the influence of temperature, pH, and chloride concentration on the pitting and crevice corrosion of UNS S30403 stainless steel. *Corrosion Science*, ***159***, p.108160.

El Hajj, H., Abdelouas, A., El Mendili, Y., Karakurt, G., Grambow, B. and Martin, C., (2013). Corrosion of carbon steel under sequential aerobic–anaerobic environmental conditions. *Corrosion Science*, ***76***, pp. 432–440.

Enning, D., Venzlaff, H., Garrelfs, J., Dinh, H.T., Meyer, V., Mayrhofer, K., Hassel, A.W., Stratmann, M. and Widdel, F., (2012). Marine sulfate-reducing bacteria cause serious corrosion of iron under electroconductive biogenic mineral crust. *Environmental Microbiology*, ***14***(7), pp. 1772–1787.

Head, I.M., Gray, N.D. and Larter, S.R., (2014). Life in the slow lane; biogeochemistry of biodegraded petroleum containing reservoirs and implications for energy recovery and carbon management. *Frontiers in Microbiology*, ***5***, p.566.

Hoffmann, K., Bienhold, C., Buttigieg, P.L., Knittel, K., Laso-Pérez, R., Rapp, J.Z., Boetius, A. and Offre, P., (2020). Diversity and metabolism of *Woeseiales* bacteria, global members of marine sediment communities. *The ISME Journal*, ***14***(4), pp. 1042–1056.

Holmkvist, L., Ferdelman, T.G. and Jørgensen, B.B., (2011). A cryptic sulfur cycle driven by iron in the methane zone of marine sediment (Aarhus Bay, Denmark). *Geochimica et Cosmochimica Acta*, ***75***(12), pp. 3581–3599.

Jones, A.A., Pilloni, G., Claypool, J.T., Paiva, A.R. and Summers, Z.M., (2021). Evidence of sporulation capability of the ubiquitous oil reservoir microbe *Halanaerobium congolense*. *Geomicrobiology Journal*, ***38***(4), pp. 283–293.

Jørgensen, B.B., (1990). The sulfur cycle of freshwater sediments: Role of thiosulfate. *Limnology and Oceanography*, ***35***(6), pp. 1329–1342.

Kaksonen, A.H. and Puhakka, J.A., (2007). Sulfate reduction-based bioprocesses for the treatment of acid mine drainage and the recovery of metals. *Engineering in Life Sciences*, ***7***(6), pp. 541–564.

Kögler, F., Dopffel, N., Mahler, E., Hartmann, F.S., Schulze-Makuch, D., Visser, F., Frommherz, B., Herold, A. and Alkan, H., (2021). Influence of surface mineralogy on the activity of *Halanaerobium sp*. during microbial enhanced oil recovery (MEOR). *Fuel*, 290, p.119973.

Lahme, S., Enning, D., Callbeck, C.M., Menendez Vega, D., Curtis, T.P., Head, I.M. and Hubert, C.R., (2019). Metabolites of an oil field sulfide-oxidizing, nitrate-reducing *Sulfurimonas sp*. cause severe corrosion. *Applied and Environmental Microbiology*, ***85***(3), pp. e01891–e01818.

Lens, P., Vallerol, M., Esposito, G. and Zandvoort, M., (2002). Perspectives of sulfate reducing bioreactors in environmental biotechnology. *Reviews in Environmental Science and Biotechnology*, ***1***, pp. 311–325.

Liang, R., Davidova, I.A., Marks, C.R., Stamps, B.W., Harriman, B.H., Stevenson, B.S., Duncan, K.E. and Suflita, J.M., (2016). Metabolic capability of a predominant *Halanaerobium sp*. in hydraulically fractured gas wells and its implication in pipeline corrosion. *Frontiers in Microbiology*, ***7***, p.988.

Lipus, D., Vikram, A., Ross, D., Bain, D., Gulliver, D., Hammack, R. and Bibby, K., (2017). Predominance and metabolic potential of Halanaerobium spp. in produced water from hydraulically fractured Marcellus shale wells. *Applied and Environmental Microbiology*, ***83***(8), pp. e02659-16.

Mitchell, M.J., Schindler, S.C., Owen, J.S. and Norton, S.A., (1988). Comparison of sulfur concentrations within lake sediment profiles. *Hydrobiologia*, *157*(3), pp. 219–229.

Mitchell, A.C., Phillips, A.J., Hamilton, M.A., Gerlach, R., Hollis, W.K., Kaszuba, J.P. and Cunningham, A.B., (2008). Resilience of planktonic and biofilm cultures to supercritical CO2. *The Journal of Supercritical Fluids*, ***47***(2), pp. 318–325.

Mori, K., Yamaguchi, K. and Hanada, S., (2018). *Sulfurovum denitrificans sp*. nov., an obligately chemolithoautotrophic sulfur-oxidizing epsilonproteobacterium isolated from a hydrothermal field. *International Journal of Systematic and Evolutionary Microbiology*, ***68***(7), pp. 2183–2187.

Mouser, P.J., Borton, M., Darrah, T.H., Hartsock, A. and Wrighton, K.C., (2016). Hydraulic fracturing offers view of microbial life in the deep terrestrial subsurface. *FEMS Microbiology Ecology*, ***92***(11).**

Murali Mohan, A., Hartsock, A., Hammack, R.W., Vidic, R.D., Gregory, K.B., (2013a). Microbial communities in flowback water impoundments from hydraulic fracturing for recovery of shale gas. *FEMS Microbiology Ecology*, ***86***, pp. 567–580. doi:10.1111/1574-6941.12183

Murali Mohan, A., Hartsock, A., Bibby, K.J., Hammack, R.W., Vidic, R.D. and Gregory, K.B., (2013b). Microbial community changes in hydraulic fracturing fluids and produced water from shale gas extraction. *Environmental Science & Technology*, ***47***, pp. 13141–13150. doi:10.1021/es402928b

Oren, A., (1999). Bioenergetic aspects of halophilism. *Microbiology and Molecular Biology Reviews*, ***63***(2), pp. 334–348.

Oren, A., 2001. The bioenergetic basis for the decrease in metabolic diversity at increasing salt concentrations: implications for the functioning of Salt Lake ecosystems. In *Saline Lakes: Publications from the 7th International Conference on Salt Lakes, held in Death Valley National Park*, California, USA, September 1999 (pp. 61–72). Springer Netherlands.

Oren, A., (2011). Thermodynamic limits to microbial life at high salt concentrations. *Environmental microbiology*, ***13***, pp. 1908–1923.

Parks, D.H., Tyson, G.W., Hugenholtz, P. and Beiko, R.G., (2014). STAMP: statistical analysis of taxonomic and functional profiles. *Bioinformatics*, ***30***(21), pp. 3123–3124.

Pyzik, A.J. and Sommer, S.E., (1981). Sedimentary iron monosulfides: Kinetics and mechanism of formation. *Geochimica et Cosmochimica Acta*, 45, pp. 687–698.

Ramana, K.V.S., Anita, T., Mandal, S., Kaliappan, S., Shaikh, H., Sivaprasad, P.V., Dayal, R.K. and Khatak, H.S., (2009). Effect of different environmental parameters on pitting behavior of AISI type 316L stainless steel: Experimental studies and neural network modeling. *Materials & Design*, ***30***(9), pp. 3770–3775.

Ravot, G., Magot, M., Ollivier, B., Patel, B.K.C., Ageron, E., Grimont, P.A.D., Thomas, P. and Garcia, J.L., (1997). *Haloanaerobium congolense sp*. nov., an anaerobic, moderately halophilic, thiosulfate-and sulfur-reducing bacterium from an African oil field. *FEMS Microbiology Letters*, ***147***(1), pp. 81–88.

Scheffer, G., Hubert, C.R., Enning, D.R., Lahme, S., Mand, J. and de Rezende, J.R., (2021). Metagenomic investigation of a low diversity, high salinity offshore oil reservoir. *Microorganisms*, ***9***(11), p.2266.

Schippers, A. and Jørgensen, B.B., (2001). Oxidation of pyrite and iron sulfide by manganese dioxide in marine sediments. *Geochimica et Cosmochi- mica Acta*, 65, pp. 915–922. doi:10.1016/S0016-7037(00)00589-5

Sindi, M. et al., (2021). Effects of extreme physicochemical parameters of injected seawater- produced water (ISW-PW) on sulfidogenesis and Microbiologically-Influenced Corrosion (MIC). In *8th International Symposium on Applied Microbiology and Molecular Biology in Oil Systems*, (p.22). Abstract Book available at: https://ismos-8.org/wp-content/uploads/2021/06/07062021_ISMOS-8_ABSTRACT-BOOKFINALFINAL.pdf

Tian, H., Yan, M., Treu, L., Angelidaki, I. and Fotidis, I.A., (2019). Hydrogenotrophic methanogens are the key for a successful bioaugmentation to alleviate ammonia inhibition in thermophilic anaerobic digesters. *Bioresource Technology*, ***293***, p.122070.

Tinker, K., Lipus, D., Gardiner, J., Stuckman, M. and Gulliver, D., (2022). The microbial community and functional potential in the Midland Basin reveal a community dominated by both thiosulfate and sulfate-reducing microorganisms. *Microbiology Spectrum*, ***10***(4), pp. e00049–e00022.

Vidal-Verdú, À. Latorre-Pérez, A., Molina-Menor, E., Baixeras, J., Peretó, J. and Porcar, M., (2022). Living in a bottle: Bacteria from sediment-associated Mediterranean waste and potential growth on polyethylene terephthalate. *Microbiology Open*, ***11***(1), p.e1259.

Viggi, C.C., Matturro, B., Frascadore, E., Insogna, S., Mezzi, A., Kaciulis, S., Sherry, A., Mejeha, O.K., Head, I.M., Vaiopoulou, E. and Rabaey, K., (2017). Bridging spatially segregated redox zones with a microbial electrochemical snorkel triggers biogeochemical cycles in oil-contaminated River Tyne (UK) sediments. *Water Research*, ***127***, pp. 11–21.

Vilcáez, J., York, J., Youssef, N. and Elshahed, M., (2018). Stimulation of methanogenic crude oil biodegradation in depleted oil reservoirs. *Fuel*, ***232***, pp. 581–590.

Widdel, F. and Bak, F., (1992). Gram-negative mesophilic sulfate-reducing bacteria. In *The Prokaryotes: A Handbook on the Biology of Bacteria: Ecophysiology, Isolation, Identification, Applications*; Balows, A., Trüper, H.G., Dworkin, M., Harder, W., Schleifer, K.-H., Eds. (pp. 3352–3378) Springer: New York, NY, USA. ISBN: 978-1-4757-2191-1.

Yao, W., and Millero, F.J., (1993). The rate of sulfide oxidation by MnO_2. *Geo- chimica et Cosmochimica Acta*, 57, p.3359–3365.

Yao, W. and Millero, F.J., (1996). Oxidation of hydrogen sulfide by hydrous Fe (III) oxides in seawater. *Marine Chemistry*, v 52, p.1–16. doi:10.1016/ 0304-4203(95)00072-0

Zhang, R., Sun, M., Zhang, H. and Zhao, Z., (2021). Spatial separation of microbial communities reflects gradients of salinity and temperature in offshore sediments from Shenzhen, south China. *Ocean & Coastal Management*, ***214***, p.105904.

Zhu, X.Y., Lubeck, J. and Kilbane, J.J., (2003). Characterization of microbial communities in gas industry pipelines. *Applied and Environmental Microbiology*, ***69***(9), pp. 5354–5363.

Zopfi, J., Ferdelman, T. and Fossing, H., (2004). Distribution and fate of sulfur intermediates–sulfite, thiosulfate, and elemental sulfur–in marine sediments. In *Sulfur Biogeochemistry–Past and Present* (pp. 97–116). Geological Society of America.